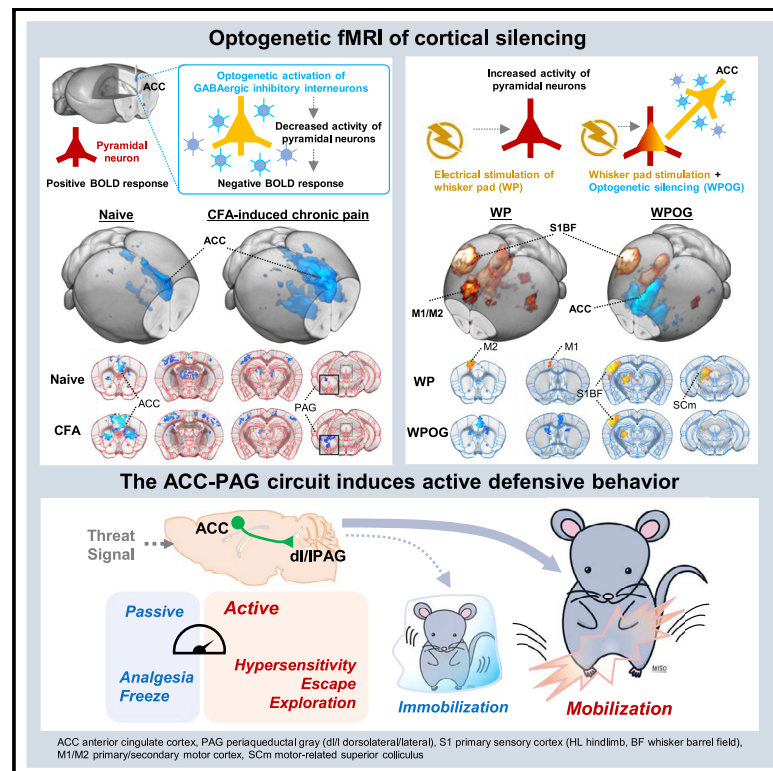


# Current Biology

## Role of anterior cingulate cortex inputs to periaqueductal gray for pain avoidance

### Graphical abstract



### Authors

Jeong-Yun Lee, Taeyi You,  
Choong-Hee Lee, Geun Ho Im,  
Heewon Seo, Choong-Wan Woo,  
Seong-Gi Kim

### Correspondence

leejy234211@gmail.com (J.-Y.L.),  
seonggikim@skku.edu (S.-G.K.)

### In brief

Using optogenetic fMRI in mice, Lee et al. reveal abnormal circuit changes of the ACC in chronic pain and identified its function to be involved in sensorimotor integration rather than sensory transmission in pain processing. In particular, the ACC-PAG circuit is vulnerable to chronic pain and induces active defensive behavior to noxious stimuli.

### Highlights

- The ACC is involved in the maintenance of chronic pain hypersensitivity
- ofMRI shows increased network strength of the ACC in the chronic pain model
- The ACC contributes to sensorimotor integration in pain processing
- The ACC-dl/IPAG circuit induces active defensive behaviors against threat signals

Article

# Role of anterior cingulate cortex inputs to periaqueductal gray for pain avoidance

Jeong-Yun Lee,<sup>1,5,\*</sup> Taeyi You,<sup>1,2,3,5</sup> Choong-Hee Lee,<sup>1</sup> Geun Ho Im,<sup>1</sup> Heewon Seo,<sup>1,4</sup> Choong-Wan Woo,<sup>1,2,3</sup> and Seong-Gi Kim<sup>1,2,3,6,\*</sup>

<sup>1</sup>Center for Neuroscience Imaging Research (CNIR), Institute for Basic Science (IBS), Suwon 16419, Republic of Korea

<sup>2</sup>Department of Biomedical Engineering, Sungkyunkwan University, Suwon 16419, Republic of Korea

<sup>3</sup>Department of Intelligent Precision Healthcare Convergence, Sungkyunkwan University, Suwon 16419, Republic of Korea

<sup>4</sup>Department of Chemistry and Biochemistry, Oberlin College, Oberlin, OH 44704, USA

<sup>5</sup>These authors contributed equally

<sup>6</sup>Lead contact

\*Correspondence: [leejy234211@gmail.com](mailto:leejy234211@gmail.com) (J.-Y.L.), [seonggikim@skku.edu](mailto:seonggikim@skku.edu) (S.-G.K.)

<https://doi.org/10.1016/j.cub.2022.04.090>

## SUMMARY

Although pain-related excessive fear is known to be a key factor in chronic pain disability, which involves the anterior cingulate cortex (ACC), little is known about the downstream circuits of the ACC for fear avoidance in pain processing. Using behavioral experiments and functional magnetic resonance imaging with optogenetics at 15.2 T, we demonstrate that the ACC is a part of the abnormal circuit changes in chronic pain and its downstream circuits are closely related to modulating sensorimotor integration and generating active movement rather than carrying sensory information. The projection from the ACC to the dorsolateral and lateral parts of the periaqueductal gray (dl/IPAG) especially enhances both reflexive and active avoidance behavior toward pain. Collectively, our results indicate that increased signals from the ACC to the dl/IPAG might be critical for excessive fear avoidance in chronic pain disability.

## INTRODUCTION

Pain is a sensory and affective experience in response to actual or potential tissue damage for survival in threatening situations. Traditionally, pain processing in the brain is known to have a sensory-discriminative dimension, which is based on the sensory information of location, quality, and an affective-motivational dimension, which establishes the unpleasantness and aversive experiences of pain.<sup>1</sup> More recently, a fear-avoidance model focused on contextual fear conditioning has been proposed to explain individual differences in chronic pain disability.<sup>1,2</sup> In these models, the context of pain determines the level of fear and the patient's attitudes to "avoidance" or "confrontation." The persistence of pain-related fear can result in the generalization of avoidance responses even in non-painful conditions, leading to chronic pain disability. However, the neural mechanisms underlying the fear avoidance of pain are poorly understood.

Defensive behaviors against fear require the selection of appropriate actions for an active or passive response. In the defense cascade model, *fight or flight* is an active defensive response to an imminent threat, enabling an organism to boost energy supplies for movement.<sup>3</sup> By contrast, *freezing* is a passive defensive response to an uncertain threat in which the "*fight or flight*" status is put on hold and motor function is halted to detect a possible threat.<sup>3</sup> In other words, if the choice between immediate avoidance and attack is difficult to determine, an organism withholds action selection.<sup>4</sup> In particular, the periaqueductal gray (PAG) coordinates the integration of sensorimotor

functions to react to a threat<sup>5</sup> and serves as the hub for descending pain control.<sup>6</sup> The dorsolateral/lateral part of the PAG (dl/IPAG) prompts active defensive responses, such as jumping and running, whereas the ventrolateral part (vlIPAG) produces analgesia and passive defensive responses, such as freezing and immobility.<sup>7</sup> However, research on the defensive behaviors toward pain has been mostly focused on the freezing response to footshock<sup>8</sup>; therefore, little is known about the active defensive responses to pain.

Functional magnetic resonance imaging (fMRI) based on blood-oxygenation-level-dependent (BOLD) signals is a noninvasive neuroimaging technique for measuring whole-brain activity. Since pain is a multidimensional experience with sensory-discriminative, affective-motivational, and cognitive-evaluative aspects involving multiple brain regions,<sup>1</sup> systems-level exploration is essential.<sup>9</sup> In human fMRI studies, correlative methods, such as functional connectivity, are powerful tools to understand pain processing at the systems level,<sup>10</sup> but they show a limited ability to provide causal interpretation.<sup>11</sup> In rodents, fMRI combined with optogenetics (ofMRI), a neuro-modulation technique that uses light-sensitive ion channels or pumps controlled by specific wavelengths, provide a unique opportunity for investigating downstream circuits in the whole brain.<sup>12</sup> Therefore, we aimed to understand neuroplasticity in chronic pain by applying ofMRI to an animal pain model.

Here, we explored the function of the anterior cingulate cortex (ACC) and its downstream circuits involved in the active defensive responses in the context of pain chronification. We focused on the ACC because it is a hub for the pain-related

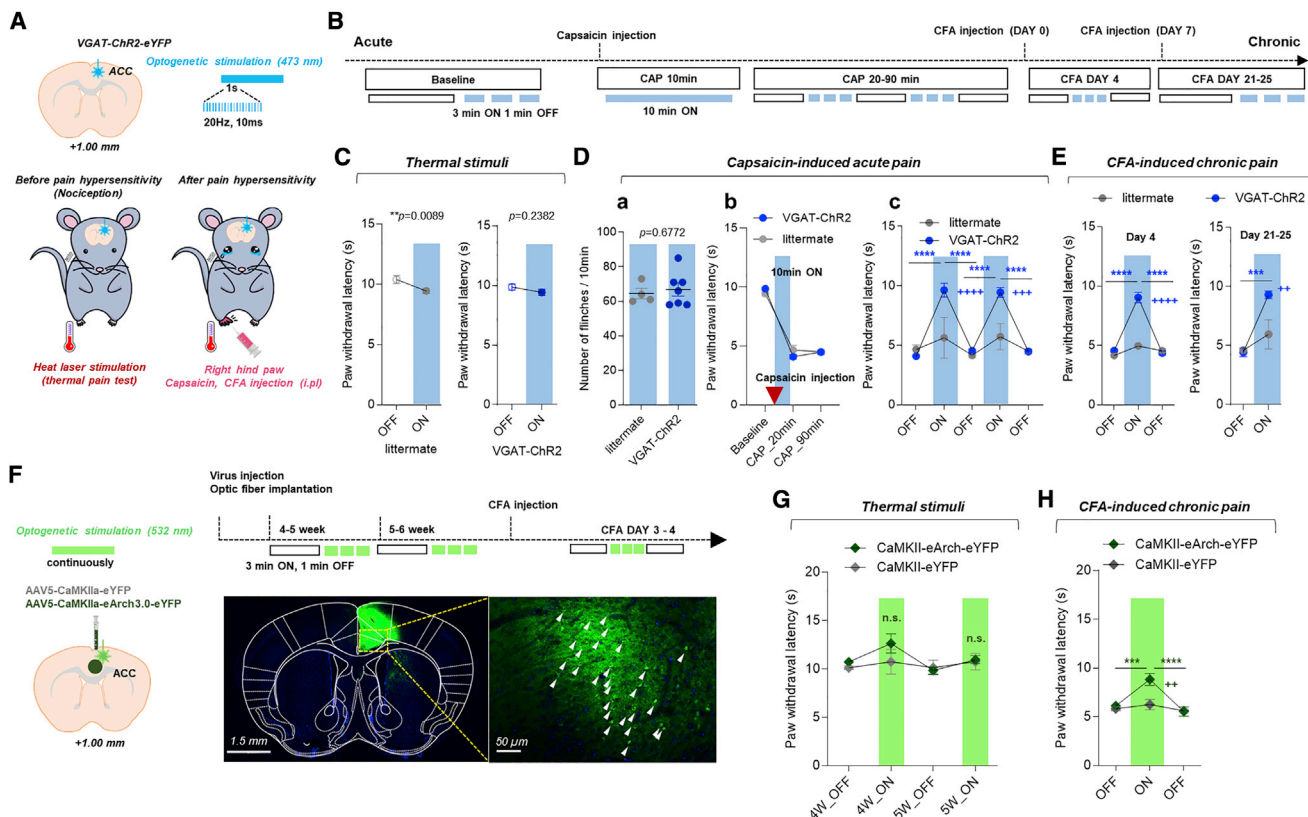


**Figure 1. Effects of the optogenetic silencing of the ACC on pain-related behavior**

(A and B) Schematic design for the experiment and experimental schedule for VGAT-ChR2 mice.

(C–E) The effect of ACC silencing on nociception (C), capsaicin-induced acute pain (D), and CFA-induced chronic pain (E); VGAT-ChR2  $n = 6-7$  and littermate  $n = 4$ .

(F) Experimental schedule and schematic design for AAV-CaMKII-eArch.

(G and H) The effect of ACC silencing on nociception (G) and CFA-induced chronic pain (H); CaMKII-eArch-eYFP  $n = 5-7$  and CaMKII-eYFP  $n = 4$ . Cross denotes significance levels compared with littermate or CaMKII-eYFP. (C paired t test, Da unpaired t test, Dc, E, G, and H two-way ANOVA.)

multidimensional experience.<sup>13</sup> In rodent studies, chronic pain changes the synaptic transmission in the ACC,<sup>14–16</sup> and the increased neural activity of the ACC engages in descending pain facilitation and fear memory formation.<sup>17–20</sup> The ACC is known to generate a teaching signal for the sources of danger and predict future dangers.<sup>21–24</sup> Our results revealed that the ACC and its downstream neural circuit are vulnerable to chronic pain. Using ofMRI at an ultrahigh field of 15.2 T, we determined that the function of the ACC is closely related to sensorimotor integration and movement generation. In particular, the ACC has numerous inputs into the dl/IPAG, and the ACC-dl/IPAG circuit modulates both reflexive and active avoidance responses to noxious stimuli.

## RESULTS

### The ACC is a part of the neural circuits associated with pain-induced neural plasticity

To examine the role of the ACC in pain processing, we observed pain-related behaviors during ACC silencing (Figure 1). The silencing of the ACC pyramidal neurons was induced by activating inhibitory interneurons or suppressing excitatory

pyramidal neurons (Figures 1A and 1F). We used transgenic mice expressing channelrhodopsin2 (ChR2) under the vesicular GABA transporter promoter (VGAT) in GABAergic interneurons (VGAT-ChR2 mice) to depolarize interneurons with light (473 nm) (Figures 1A–1E) or an adeno-associated virus (AAV) expressing archaerhodopsin (Arch) under a calcium/calmodulin-dependent protein kinase II (CaMKII) promoter to hyperpolarize excitatory pyramidal neurons with light (532 nm) (Figures 1F–1H). The thermal pain threshold was estimated by measuring the reflexive paw withdrawal latency under infrared stimulation. To investigate the role of the ACC in the transition from nociception to chronic persistent pain, we injected capsaicin (CAP) for acute pain and complete Freund's adjuvant (CFA) for chronic pain into the hind paw. In the animal pain model, it is known that persistent pain for 3 weeks induces changes in brain circuitry, leading to anxiety and decreased motivation.<sup>25,26</sup> Thus, we injected CFA twice to prolong the CFA-induced persistent pain for more than 3 weeks.

The optogenetic activation of GABAergic interneurons (VGAT-ChR2, 3–5 mW, 20 Hz, and 10 ms) in the cortex can depolarize interneurons and consequently hyperpolarize excitatory pyramidal neurons.<sup>27,28</sup> The optogenetic activation of ACC<sup>VGAT</sup> neurons

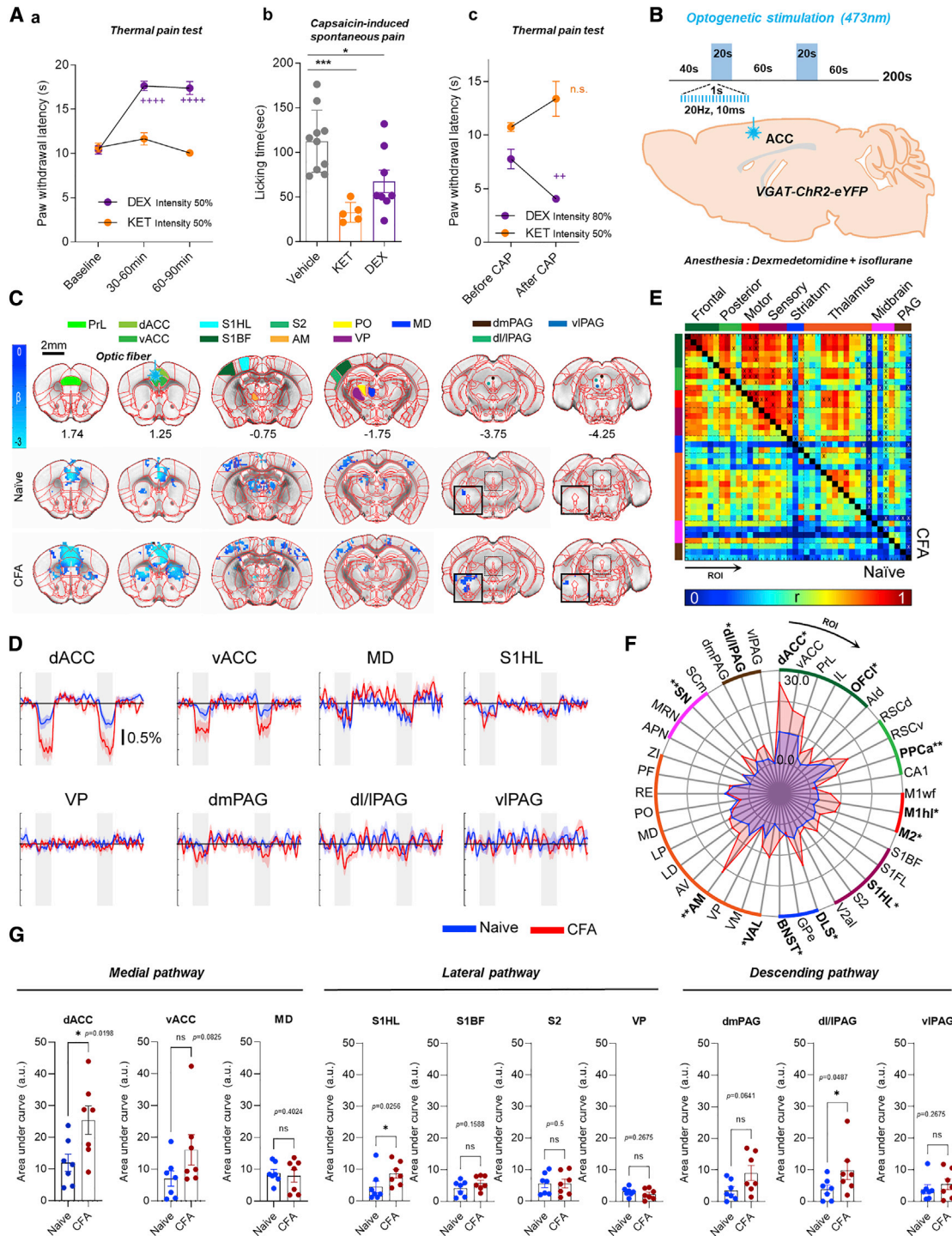


**Figure 2. Brain-wide BOLD fMRI during optogenetic silencing of ACC in naive and CFA-induced chronic pain model**

(A) The effect of ketamine (KET) and dexmedetomidine (DEX) on the thermal pain threshold (a), capsaicin (CAP)-induced spontaneous pain (b), and pain hypersensitivity (c); vehicle n = 10, KET n = 5–6, and DEX n = 7.

(B) Experimental design for ofMRI; naive n = 7 and CFA n = 7.

(C) Group activation maps of naive and CFA mice during ACC inhibition; Z > 2.8, cluster corrected at p = 0.05. To visualize PAG activity, maps were generated with a threshold of Z > 1.96, cluster corrected at p = 0.05, and presented as insets.

(D) Time courses of BOLD fMRI in representative ROIs.

(E) Connectivity matrix of all responsive ipsilateral ROIs. × denotes significance of p = 0.05 family-wise error rate (FWER) corrected for multiple comparisons.

(legend continued on next page)

did not affect the thermal pain threshold in naive mice (Figure 1C). Similarly, the optogenetic inhibition of ACC<sup>CaMKII</sup> neurons caused no change in the thermal pain threshold (Figure 1G). To examine whether ACC suppression influences spontaneous pain and pain hypersensitivity, ACC<sup>VGAT</sup> neurons were immediately activated for 10 min after CAP injection. The silencing of the ACC failed to block the CAP-induced spontaneous pain behavior and the induction of pain hypersensitivity (Figures 1Da and 1Db). However, the activation of ACC<sup>VGAT</sup> neurons reversed the maintenance of CAP- or CFA-induced pain hypersensitivity (Figures 1Dc and 1E). Similarly, the optogenetic inhibition of ACC<sup>CaMKII</sup> neurons blocked pain hypersensitivity in the CFA-induced chronic pain model (Figure 1H). Thus, the ACC is engaged in the maintenance of pain hypersensitivity rather than nociception.

### The ACC and its downstream circuit are involved in chronic pain

To explore the spontaneous neural activity of the ACC and its downstream circuits, we performed optogenetic silencing fMRI under light anesthesia (Figure 2).<sup>29</sup> Since anesthesia can suppress pain circuits, we investigated the effect of anesthesia on pain behaviors at a subanesthetic dose of ketamine (KET) and dexmedetomidine (DEX) (Figure 2A), which are suitable for mouse fMRI.<sup>30</sup> Unlike KET, DEX suppressed nociception (Figure 2Aa) but did not block pain hypersensitivity (Figure 2Ac). Therefore, we chose DEX to investigate the role of the ACC in pain hypersensitivity.

Both activations of ACC<sup>VGAT</sup> neurons and inhibition of ACC<sup>CaMKII</sup> neurons caused negative BOLD responses (Figures 2 and S1). Since silencing the excitatory pyramidal neurons by the stimulation of VGAT interneurons is more effective than that by the optogenetic inhibition of CaMKII neurons,<sup>27</sup> we chose to focus on the ofMRI of VGAT-ChR2 mice. To investigate the circuit changes caused by chronic pain, we compared the ofMRI responses in naive mice and the CFA-induced chronic pain model ( $\geq 3$  weeks after CFA injection). The activation of ACC<sup>VGAT</sup> neurons caused larger negative BOLD responses in the ACC and several downstream regions of the CFA-induced chronic pain model compared with the naive mice (Figures 2C–2G and S2). Moreover, the functional connectivity strength between all the responsive regions of interest (ROIs) was enhanced in the CFA-induced chronic pain model (Figure 2E). Despite the controversy regarding the origin of negative BOLD responses,<sup>31</sup> the appearance of these responses in optogenetic silencing fMRI reflects the deactivation of excitatory pyramidal neurons at the target region.<sup>29</sup> The amplitude of the fMRI signal reduction is closely dependent on a reduction in the spontaneous neural activity from baseline.<sup>32</sup> Since ACC silencing suppresses the excitatory output to downstream pathways, the magnitude of the downregulated neuronal activity reflects the degree of inter-regional communication under basal conditions. Thus, persistent pain increases the spontaneous neural activity of the ACC

and interconnected network strength of downstream regions such as the lateral pathway for a sensory-discriminative pain (primary somatosensory hindlimb cortex [S1HL]), the medial pathway for an affective-motivational pain (the ACC and medial dorsal thalamus [MD]), the descending pathway (PAG), and the motor-related system (primary motor hindlimb cortex [M1h], secondary motor cortex [M2], and ventral anterolateral thalamus [VAL]) (Figures 2D, 2F, and 2G).

### The ACC is involved in sensorimotor integration in pain processing

To further dissect the downstream circuits of the ACC for pain processing, we combined the optogenetic silencing of the ACC with electrical stimuli (Figure 3). Electrical stimulation (4 Hz) is transmitted as a noxious signal (Figure S3). Noxious electrical stimulation of the whisker pad (WP) showed a stable positive BOLD response in the pain pathway and sensorimotor-related brain regions (Figures 3B–3F). The modularity-based community detection of the functional connectivity patterns identified two modules: WP-related and polymodal ROIs (Figure 3D). WP-related ROIs are areas directly related to the whisker somatosensory network, as described previously.<sup>30,33</sup> When noxious stimulation was combined with optogenetic ACC silencing (WPOG, WP and optogenetic stimulation), BOLD amplitudes were reduced by the ACC-modulated downstream circuits (Figures 3B–3F). The inter-region connectivity matrix was grouped into three functional modules (Figure 3D): (1) WP-dominant ROIs (WP-d), which did not have a significant modulation from ACC silencing, primarily make up somatosensory regions such as primary somatosensory barrel field (S1BF) and ventral posterior thalamus (VP); (2) ACC-dominant ROIs (ACC-d) with no WP response have a significant negative BOLD response, creating a negative correlation; and, (3) importantly, optogenetic ACC silencing significantly reduced noxious stimulation-induced BOLD responses in ACC-modulated areas (ACC-m), including the descending pain pathway (dl/IPAG and vlPAG) and motor-related pathways (M2, M1, and superior colliculus motor region [SCm]) (Figures 3C–3F). These data indicate that the downstream targets of the ACC are closely related to sensorimotor integration and movement generation rather than sensory discrimination in pain processing.

Next, to examine the efferent projections of the ACC, we injected an anterograde viral tracer (AAV5) expressing eYFP under the CaMKII promoter into the ACC (Figure 4A). Anterograde labeling showed dense projection from the ACC to the neural circuits for defensive behaviors such as PAG and SCm,<sup>8,34,35</sup> whereas somatosensory circuits such as S1, S2, and VP received less input from the ACC (Figures 4A and S4A). Compared with anterograde monosynaptic tracing, which represents only direct presynaptic input, ofMRI can reveal brain activity by multisynaptic pathways. The optogenetic activation of ACC<sup>CaMKII</sup> neurons induced a positive BOLD response throughout the brain regions, but the magnitude of the BOLD signal was dependent on the

(F and G) Absolute area under the curve (AUC) of the BOLD response in each ROI; mean (F) and individual data (G).

Ordering of ROIs in (F) denotes ordering in (E). ROI abbreviations: see STAR Methods.

Cross denotes significance levels in comparison with baseline or before CAP. (Aa and Ac: two-way ANOVA, Ab: one-way ANOVA, E: unpaired t test, F and G: Mann-Whitney U test.)

See also Figures S1 and S2.

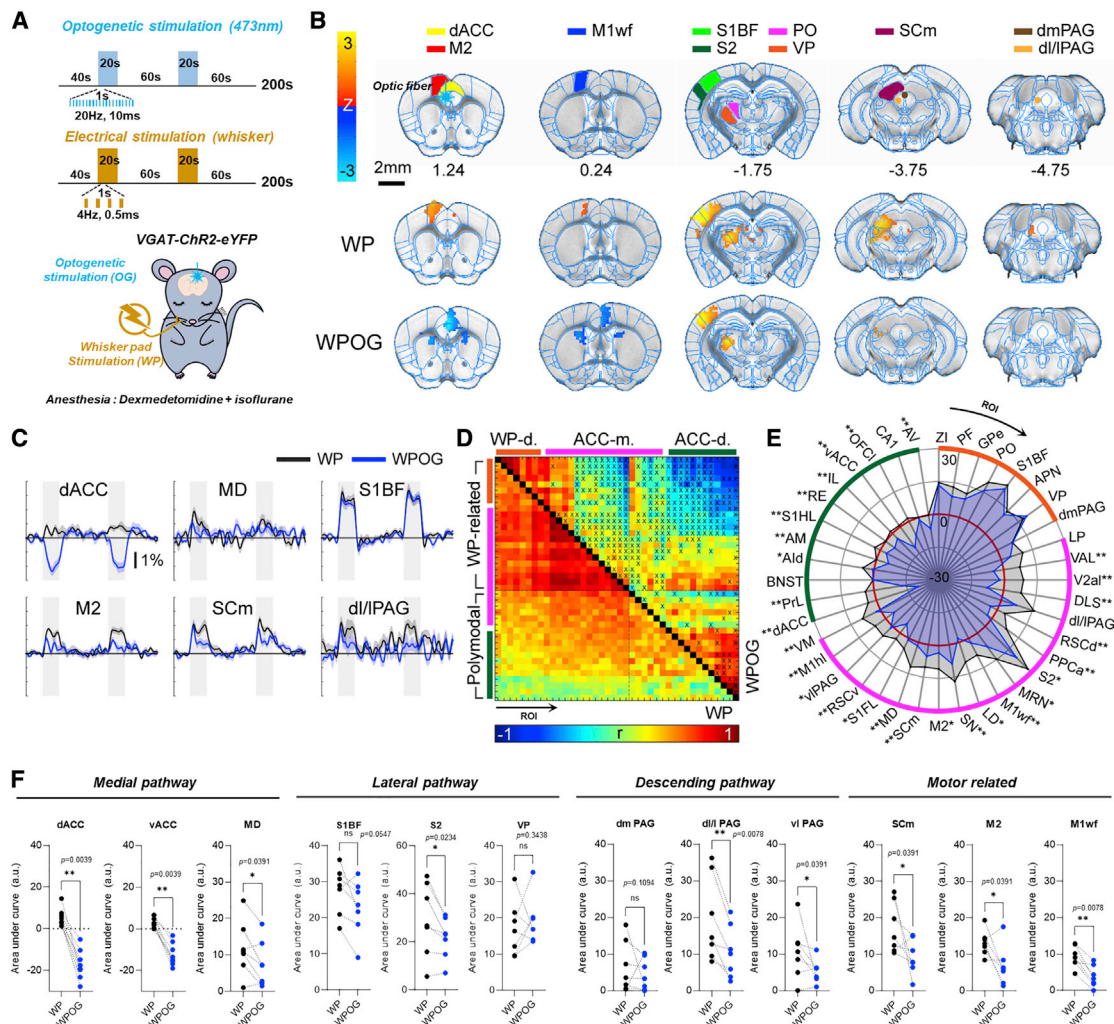


**Figure 3. Effects of ACC silencing on the BOLD responses induced by the noxious electrical stimulation of whisker pad**

(A) Experimental design for silencing of mMRI combined with electrical stimulation.  
 (B) Group activity maps from the noxious stimulation of whisker pad (WP) without and with optogenetic ACC silencing (WPOG);  $Z > 2.8$ , cluster corrected at  $p = 0.05$ .  
 (C) Time courses of BOLD fMRI in representative ROIs.  
 (D) Connectivity matrix of all responsive ROIs.  $\times$  denotes  $p = 0.05$  FWER; two modules in WP (WP-related, polymodal,) and three modules in WPOG were classified (WP-d, WP dominant, ACC-m, ACC modulated, and ACC-d, ACC dominant).  
 (E and F) AUC of the WP-induced BOLD response without and with optogenetic silencing; ROI order in (E) denotes the order in (D). Mean (E) and individual data (F);  $n = 7-8$ . (D: paired t test; E and F: Wilcoxon test.)  
 See also [Figure S3](#).

strength of the synaptic activity.<sup>36</sup> The BOLD signal decreased with increasing distance from the stimulated ACC region (rostral to caudal), and a significant difference was observed between the *ipsilateral* and *contralateral* thalamus regions (Figure 4Ca). At a high threshold, the optogenetic activation of ACC<sup>CaMKII</sup> neurons showed BOLD activation patterns in the brain regions receiving direct input from the ACC (Figure 4B). Similar to the viral tracing of ACC<sup>CaMKII</sup> neurons, the optogenetic activation of ACC<sup>CaMKII</sup> neurons induced a higher BOLD response in the dl/IPAG than in S1 (Figure 4Cb). Similarly, the BOLD response of the dl/IPAG, although not significant, was also higher than those of the vlPAG and dmPAG (Figure 4Cb). In accordance, the activation of

ACC<sup>VGAT</sup> neurons showed that a stronger inhibition was found in the ACC and dl/IPAG compared with S1 or VP (Figure 2). Collectively, our results suggest that the function of the ACC is closely related to the dl/IPAG regions.

In addition to the ACC, the prelimbic cortex (PrL) also belongs to the medial frontal cortex (MFC) in rodents. In the chronic pain model, decreased input from the PrL to the vlPAG induces pain hypersensitivity.<sup>37-39</sup> Thus, we determined the innervation site of the PAG from the ACC and the PrL (Figures 4D, S4B, and S4C). The vlPAG received dense input from the PrL rather than the ACC, whereas the dl/IPAG received dominant inputs from the ACC.

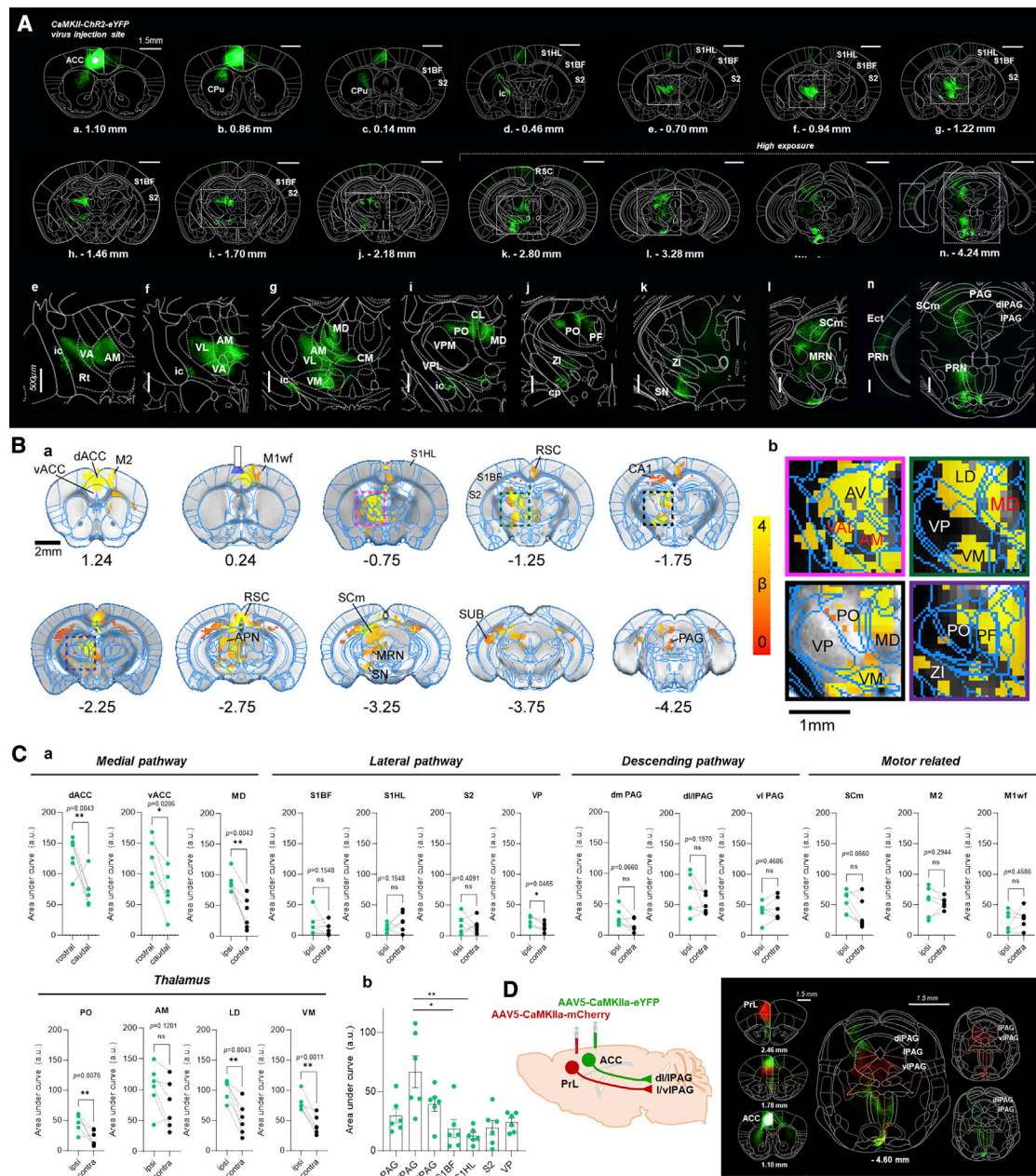


**Figure 4. Efferent projections of the ACC and functional connections under the optogenetic activation of the ACC**

(A) Whole-brain tracing maps of the axonal projections from the ACC neurons with distances relative to bregma; subcortical sections indicated by dashed boxes were expanded for better visualization.

(B) Mean BOLD activation maps induced by the optogenetic activation of the ACC<sup>CaMKII</sup> neurons with distances relative to bregma; Z > 3.29, cluster corrected at p = 0.05. The dashed boxes were used for expansion in (b).

(C) AUC of the BOLD response in ROIs during the activation of ACC<sup>CaMKII</sup> neurons (a), and the comparison of fMRI responses in ipsilateral ROIs (b); n = 6.

(D) Anterograde tracing from the PrL or ACC into subregions of the PAG. (Ca Mann-Whitney U test and Cb Kruskal-Wallis test.)

See also Figure S4.

### The ACC projection to the PAG contributes to pain behavior

To assess the function of the ACC-PAG circuit, we injected an anterograde virus containing the CaMKII promoter with Chr2 or Arch into the ACC and modulated the axon terminal in the dl/IPAG with light (Figure 5). The optogenetic activation of the

ACC-PAG circuit decreased the thermal pain threshold (Figure 5B), whereas the optogenetic inhibition increased the thermal pain threshold in naive mice and suppressed CFA-induced pain hypersensitivity (Figure 5D). Additionally, KET (NMDA receptor antagonist) partially blocked the pain hypersensitivity in the hind paw contralateral to the optogenetically

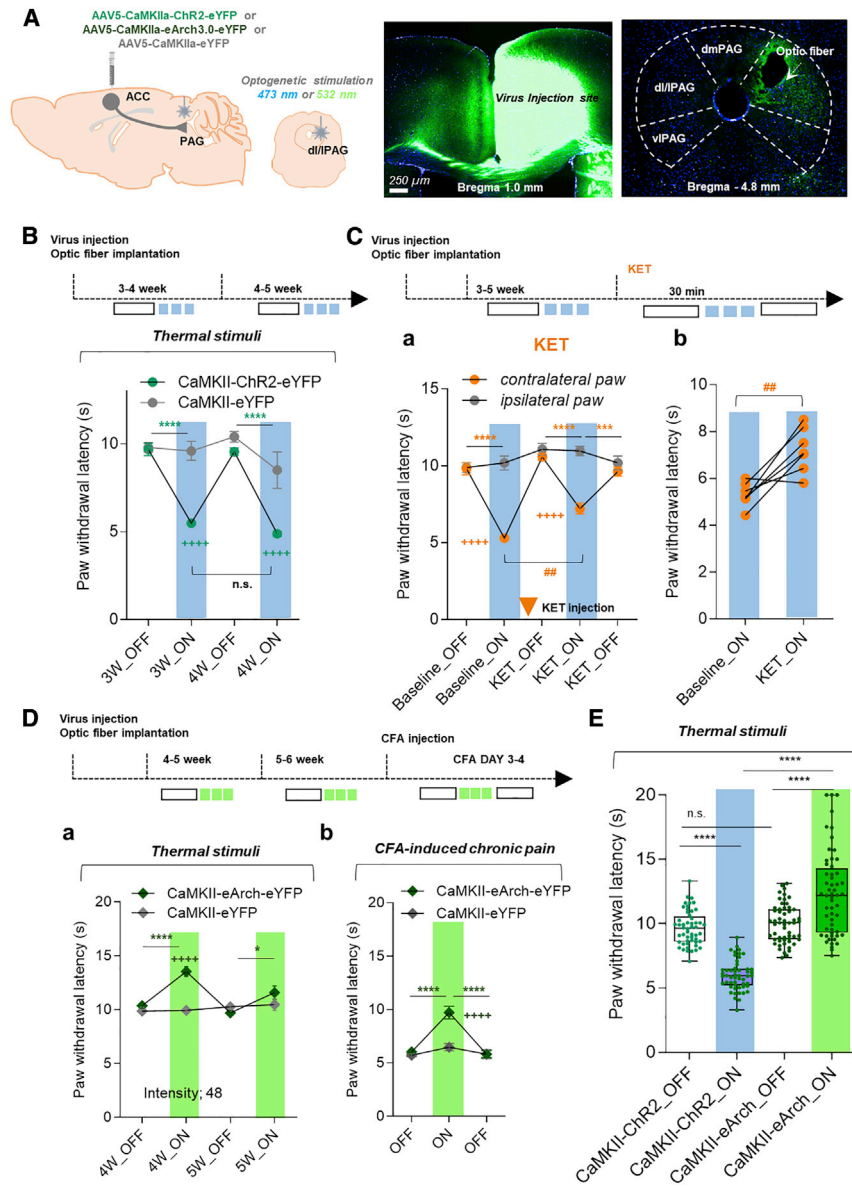


**Figure 5. Effects of the optogenetic modulation of the ACC-PAG inputs on pain-related behavior**

(A) Circuit-specific modulation scheme and histological confirmation. (B) The effect of the optogenetic activation of ACC-PAG on the thermal pain threshold at 3–4 weeks (3W) or 4 to 5 weeks (4W) after virus injection; CaMKII-ChR2-eYFP  $n = 7$  and CaMKII-eYFP  $n = 6$ . (C) The effect of ketamine on pain hypersensitivity by the activation of ACC-PAG; contralateral/ipsilateral paw in relation to the transfected pathway. Individual data comparing before (baseline) and after ketamine injection (KET) (b);  $n = 7$ . (D) The effect of the optogenetic inhibition of ACC-PAG on the thermal pain threshold (a) and the CFA-induced chronic pain (b); CaMKII-eArch-eYFP  $n = 5–7$  and CaMKII-eYFP  $n = 4$ . (E) The effect of bidirectional modulation of ACC-PAG on the thermal pain threshold. Thermal latency was measured 4 or 8 times in 7 mice at each condition and plotted together. Cross denotes significance levels in comparison with CaMKII-eYFP or ipsilateral paw. (B–D: two-way ANOVA and E: one-way ANOVA.) See also Figure S5.

activated ACC-PAG circuit (Figure 5C), indicating glutamatergic synaptic neurotransmission.

Pain behavior can be enhanced by anxiety, which is closely related to the ACC.<sup>13</sup> Thus, we examined whether the ACC-PAG circuit is associated with the anxiety level by using an open-field test (Figures 6A, 6B, and S5A). As anxiety levels increased, mice showed reduced exploratory behavior and locomotion and avoided the center zone. During the optogenetic activation of the ACC-PAG circuit, the speed of movement increased without abnormal motor behavior (Video S1), but the time spent in the center zone did not change (Figure 6B). On the other hand, the optogenetic inhibition of the ACC-PAG circuit decreased the duration in the center zone (Figure S5A). Therefore, the ACC-PAG circuit is unlikely to cause pain hypersensitivity by increasing the anxiety levels.

### The ACC projection to the PAG contributes to fear response

We next investigated the role of the ACC-PAG in innate fear response by using fox urine (Figures 6C, 6D, and S5B). The optogenetic activation of the ACC-PAG circuit increased the speed of movement, similar to the results of the open-field test (Figure 6Da), whereas the optogenetic inhibition of the ACC-PAG circuit slightly decreased the speed of movement (Figure S5Bc). After exposure to predator odors, mice avoided the places with odors (zone 1). After 2 min, the continuous exposure to predator odor alleviated the avoidance behavior toward zone 1 (Figures 6Db and S5B). Zone 2 (away from odors) preference was still high in the control and ACC-PAG inhibition groups, but the ACC-PAG activated (CaMKII-ChR2-eYFP) mice preferred to be in zone 1 (Figure S5Bd). Thus, in an uncertain threat, the increased input from the ACC to PAG induces active movement related to exploratory behavior toward the threat environment.

Finally, we examined the role of the ACC-PAG circuit in learned fear response to noxious stimuli with an active place avoidance task (APAT) (Figures 6E–6H). In the APAT, mice receive electrical shocks whenever they enter a certain section (60° shock zone) on a counterclockwise rotating platform. After learning the shock zone location via spatial cues, mice freely and actively avoid the shock zone. Before the optogenetic experiment (day 1), mice were trained to avoid a 60° shock zone, and the number of shocks was counted to ensure that the mice learned the shock zone (Figure 6G). On day 2, the

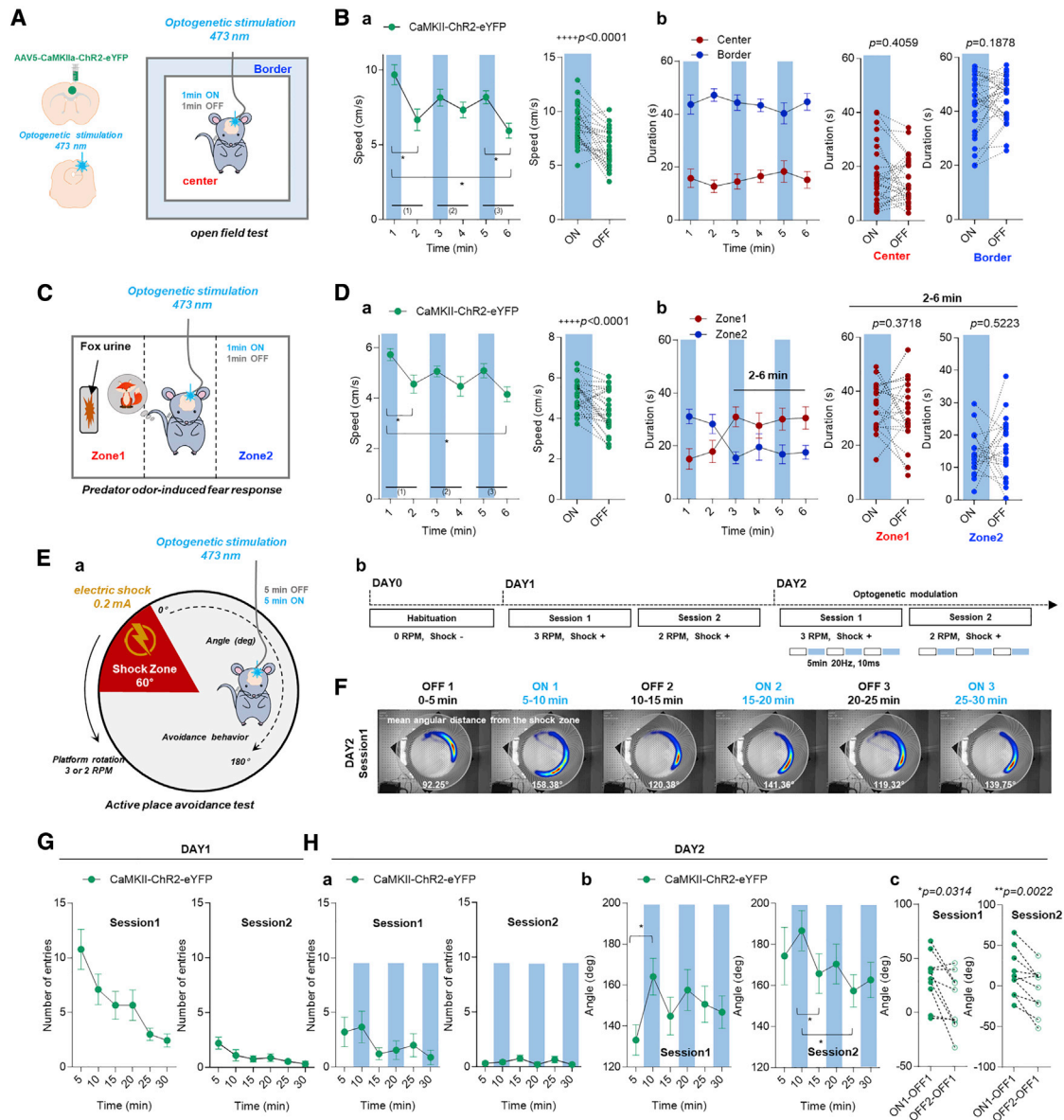


**Figure 6. Effects of the optogenetic activation of ACC-PAG inputs on anxiety, innate fear, and active avoidance response**

(A) Experimental design for the open-field test.

(B) The effect of the optogenetic activation of ACC-PAG on the speed of movement (a) and the duration in center/border zone (b);  $n = 9$ .

(C) Experimental design for the innate fear response induced by fox urine.

(D) The effect of the optogenetic activation of ACC-PAG on the speed of movement (a) and the durations spent in zone 1 and zone 2 (b);  $n = 9$ .

(E) Experimental design (a) and schedule (b) for active place avoidance task.

(F) Representative heat map of time spent.

(G) Number of entries into the shock zone on day 1.

(H) The effect of the optogenetic activation of ACC-PAG on the number of entries into the shock zone (a) and the angle from the shock zone (b and c) on day 2;  $n = 9-10$ .

Ba, Da, and Hb: repeated measures one-way ANOVA and B, D, and Hc: paired t test.)

See also [Figures S5](#) and [S6](#) and [Videos S1](#) and [S2](#).

number of shocks was close to zero and independent of the optogenetic activation of the ACC-PAG circuit ([Figure 6Ha](#)). Interestingly, in one mouse that received multiple shocks on day 1, the optogenetic activation of the ACC-PAG circuit decreased the number of shocks ([Figure S6](#)). To avoid shock, mice showed a clockwise running behavior, so the angle

of their position was measured from the shock zone ([Figures 6Hb](#) and [6Hc](#)). The optogenetic activation of the ACC-PAG circuit increased the angle from the shock zone ([Figures 6F](#), [6Hb](#), and [6Hc](#)). These data indicate that increased inputs from the ACC to PAG contribute to active avoidance behavior to noxious stimuli.

## DISCUSSION

In this study, we demonstrate the function of the ACC for active defensive response in pain processing. We found that the ACC is a part of neural circuits associated with pain-induced neural plasticity. The downstream circuit of the ACC is closely related to the dl/IPAG, which is a key region for active defensive response. The activation of the ACC-dl/IPAG circuit enhances both reflexive and active avoidance behavior. Our results suggest that increased input from the ACC to the PAG might be a critical factor for abnormal circuit changes in chronic pain.

### The role of the ACC in pain chronification and fear formation

The ACC receives direct nociceptive inputs and encodes the unpleasantness of pain.<sup>13</sup> In both animal and human studies, the activity in the ACC correlates with the intensity of acute pain stimuli,<sup>40,41</sup> and chronic persistent pain causes hyperactivity in the excitatory pyramidal neurons of the ACC.<sup>40,42,43</sup> Since the optogenetic activation of GABAergic interneurons in the cortex suppresses the spontaneous activity of excitatory pyramidal neurons, the resulting negative BOLD response reflects baseline activity.<sup>28,29</sup> In our data, the negative BOLD response after ACC silencing was greater in the chronic inflammatory pain model (Figure 2), suggesting that the baseline neural activity of the excitatory pyramidal neurons in the ACC increased from chronic persistent pain.

In rodent studies, both electrical stimulation and chemical activation of the glutamate receptors in the ACC produced a pronociceptive and aversive response.<sup>17–20,44,45</sup> Compared with electrical and chemical activation, optogenetic stimulation has the advantage of modulating specific cell types at precise time windows. The optogenetic activation of the ACC pyramidal neurons (CaMKII or Thy1) facilitates pain-related behaviors.<sup>46,47</sup> Consistent with previous studies,<sup>47,48</sup> our study showed that direct (via CaMKII-eArch) and indirect (via VGAT-ChR2) inhibition of the ACC pyramidal neurons selectively suppresses pain hypersensitivity without affecting nociception (Figure 1). Furthermore, the modulation of the glutamatergic synaptic plasticity in the ACC was sufficient to relieve chronic pain without affecting nociception.<sup>49–51</sup> Thus, the ACC pyramidal neurons are important for synaptic alteration of chronic pain.<sup>13</sup>

The artificial activation of the ACC also induces fear experience even without aversive stimuli.<sup>18,19</sup> The inhibition of the ACC during the fear-acquisition phase does not impair nociception or innate fear response but reduces the fear response during the fear-expression phase.<sup>18,52</sup> Furthermore, the ACC is responsible for paying attention to pain-related signals.<sup>23,24,53</sup> In trace fear conditioning with a time gap between footshock and a conditioned stimulus, distraction interferes with the formation of the fear experience, so the attentional role of the ACC is essential in trace fear.<sup>24,54</sup> This evidence suggests that the functional plasticity of the ACC generates a teaching signal for aversive experiences and is engaged in fear formation.

### The role of the frontal cortical projections to the PAG in pain and fear response

The PAG is a critical hub for the descending pain modulatory system, originating in the brainstem and regulating the pain

signals at the spinal cord.<sup>6</sup> Since the activation of the ACC modulates the nociceptive input at the spinal cord,<sup>17,20,55</sup> the ACC-dl/IPAG circuit may engage in descending pain facilitation. Consistent with previous studies,<sup>52,56</sup> our anterograde tracing showed that the ACC densely innervates the dl/IPAG (Figures 4 and S4). The silencing of the ACC in the CFA-induced chronic pain model shows an increase in the network strength of its downstream regions, such as the dl/IPAG (Figure 2). Previous studies have suggested that the ACC-PAG synapse is glutamatergic.<sup>57,58</sup> Injection of a retrograde tracer into the PAG followed by immunohistochemical staining indicates that the retrogradely labeled neurons in the ACC contain glutamate-like immunoreactivity.<sup>57</sup> Moreover, pharmacological approaches have demonstrated that the ACC is one of the glutamatergic inputs to the PAG.<sup>58</sup> In this study, the activation of the ACC-dl/IPAG induced pain hypersensitivity, whereas KET reduced this pain hypersensitivity (Figure 5), indicating glutamatergic synaptic neurotransmission.

In fear response, the neural activity in the ACC is closely related to terminate freezing.<sup>23,59</sup> Exploratory behavior is necessary for recognizing the safety and dangers of the environment, which affects avoidance decisions. In the presence of a persistent threat signal, the activation of the ACC-dl/IPAG circuit enhanced exploratory behavior toward predator odor (Figures 6D and S5B). Therefore, when an uncertain threat persists, the ACC-PAG circuit induces an active response rather than a passive response withholding the action selection. In learned fear response to noxious stimuli with APAT, the activation of ACC-dl/IPAG also enhanced the avoidance behavior toward the approaching footshock zone (Figure 6H). Therefore, the ACC-dl/IPAG circuit is involved in both pain and active defensive responses.

The intrinsic excitability of PrL endogenously suppresses pain and anxiety.<sup>39,60,61</sup> In the chronic pain model, in contrast to the increased activity of the ACC, the excitability of PrL is decreased,<sup>39,60</sup> and decreased inputs from the PrL to vlPAG are critical for the development of chronic pain.<sup>37–39</sup> Thus, the PrL and ACC project into different subregions of the PAG with opposing actions in pain and defensive behavior (Figures 4D and S4), suggesting that the frontal cortical projections to the PAG are important for pain and defensive response.

### Relevance to pain fMRI studies in humans

The human MFC, which consists of the ACC and the medial prefrontal cortex (mPFC), is a key structure for pain, negative emotion, and cognitive control.<sup>62</sup> The rodent MFC has been a controversial issue since granular parts, which are critical for high-level cognitive function in human mPFC, do not exist.<sup>63</sup> The Brodmann classification divided the cerebral cortex based on a cytoarchitectural organization of cells, such as the granular layer. By the Brodmann nomenclature, the rodent ACC (Area 24) appears to be homologous to the human dACC or anterior mid-cingulate cortex (amCC) regions and the rodent PrL (Area 32) to the human pgACC.<sup>64</sup> In human fMRI studies, imminent danger requiring active avoidance increases the activity in the dACC and dACC-PAG connectivity, whereas high shock probability increases the activity in the pgACC.<sup>65</sup> Furthermore, pain-related prediction errors lead to the selection of actions expected to have a low probability of pain in which the failure to avoid pain

due to incorrect prediction causes higher activity in aMCC and PAG.<sup>66</sup> Cognitive tasks such as visual attention produce attentional analgesia, which involves the ACC and PAG.<sup>67–69</sup> Given that the ACC is activated by both reward and pain to generate attention for learning and prediction,<sup>70–72</sup> attention reallocation in the context of pain is likely to be involved in defensive responses. In this study, we proposed a hypothesis for different connections of ACC subregions to PAG (dACC-dl/IPAG versus pgACC-vIPAG) and their different roles in defensive responses in pain processing (Figure S4), which is worthy of future study by human fMRI.

### The role of the ACC in motor output

The ACC is known to engage in shaping the motor output based on the sensory input related to expected reward or punishment.<sup>23,73–75</sup> In this study, the modulatory effect of the ACC was pronounced in motor-related systems (Figures 2 and 3). In particular, the SCm is essential for the integration of sensorimotor function and the transmission of visual threat signals,<sup>34,76,77</sup> and the ACC-SC circuit is known to coordinate specific action selection.<sup>78</sup> The ACC has dense projections to the SCm (Figure 4), and noxious stimuli induce a positive BOLD response in SCm, which is modulated by the optogenetic silencing of ACC (Figure 3). Therefore, our data suggest that the ACC-SC circuit may be involved in pain-related defensive behavior.

The nigro-striatal-thalamocortical network, which includes the substantia nigra (SN), dorsal lateral striatum (DLS), VAL, and M1/M2, constitutes a key pathway in motor integration and execution.<sup>79–81</sup> The ACC has a dense input to the nigro-striatal-thalamocortical network (Figure 4), and chronic pain appears to enhance the network strength of these downstream regions (Figure 2E). Furthermore, the optogenetic silencing of the ACC significantly reduced the noxious stimulation-induced BOLD responses in the nigro-striatal-thalamocortical network (Figure 3E). Thus, the ACC seems to have a critical role in the motor output related to pain processing.

The function of PAG also is closely related to the motor cortex.<sup>82,83</sup> However, during the unilateral modulation of the ACC-PAG circuit, we did not observe any abnormal motor behavior such as contralateral rotations (full 360° turns) related to the motor cortex<sup>84</sup> (Videos S1 and S2). Furthermore, the modulation of the ACC-PAG circuit did not affect the speed of movement (i.e., the movement distance) compared with the control group in the open-field test, whereas the optogenetic inhibition significantly decreased movement distance in the innate fear test (Figure S5). Thus, the effect of the ACC-PAG circuit on locomotion seems to be associated with the affective aspect rather than the direct activation of the motor system.

### Potential targets for pain processing

The ACC is also involved in the motivation for goal-directed or effortful behavior.<sup>85,86</sup> In particular, the nucleus accumbens (NAc) is a key region for decreased motivation in chronic pain,<sup>25</sup> and the ACC-NAc circuit modulates pain and fear responses.<sup>87,88</sup> In our study, ofMRI allowed the identification of other potential target brain regions. Enhanced response in the bed nucleus of the stria terminalis (BNST) and the lateral orbitofrontal cortex (OFCI) was detected in the chronic pain

model (Figure 2F). BNST activity regulates pain aversion, with recent studies hypothesizing its involvement in goal-directed defensive response.<sup>89,90</sup> Ventrolateral OFC's (OFCvI) role in anti-nociception is well reported, with little known about the OFCI's involvement aside from its roles in decision making and valence integration.<sup>91–93</sup> Taken together, these areas may provide motivational and cognitive control of pain with the ACC.

Finally, to our surprise, the anteromedial thalamus (AM) showed the second-highest response in the chronic pain model (Figure 2F). The AM reacts to predator and social threats<sup>94,95</sup> and has reciprocal connections with the ACC, which contribute to contextual fear memory.<sup>52,96</sup> However, since the AM did not respond to noxious stimulation (Figure 3E), further studies are needed to determine the role of AM in pain chronification.

In conclusion, our findings offer insights into the neural mechanisms underlying the fear-avoidance response to pain, a key factor for chronic pain disability. Furthermore, we sought to apply ofMRI to explore pain circuits at the systems level, which will provide a much-needed avenue for pain research.

### STAR★METHODS

Detailed methods are provided in the online version of this paper and include the following:

- KEY RESOURCES TABLE
- RESOURCE AVAILABILITY
  - Lead contact
  - Materials availability
  - Data and code availability
- EXPERIMENTAL MODEL AND SUBJECT DETAILS
  - Animals
- METHOD DETAILS
  - Stereotaxic surgery
  - Optogenetics
  - Behavior tests
  - MRI
  - Viral tracing
- QUANTIFICATION AND STATISTICAL ANALYSIS
  - Behavior analysis
  - GLM statistical mapping
  - BOLD quantification
  - Functional connectivity analysis

### SUPPLEMENTAL INFORMATION

Supplemental information can be found online at <https://doi.org/10.1016/j.cub.2022.04.090>.

### ACKNOWLEDGMENTS

This project was funded by the Institute for Basic Science in Korea (IBS-R015-D1 to S.-G.K.).

### AUTHOR CONTRIBUTIONS

S.-G.K. obtained funding for the study and guided the project. J.-Y.L., T.Y., and G.H.I. conducted the ofMRI experiments, collected data, and analyzed the results. J.-Y.L., C.-H.L., and H.S. conducted the behavior experiments, collected data, and analyzed the results. J.-Y.L. conducted histological

experiments. J.-Y.L., T.Y., C.-W.W., and S.-G.K. wrote the manuscript. C.-W.W. and S.-G.K. supervised the study. All the authors reviewed the manuscript and gave final approval.

#### DECLARATION OF INTERESTS

The authors declare no competing interests.

Received: December 7, 2021

Revised: March 7, 2022

Accepted: April 28, 2022

Published: May 23, 2022

#### REFERENCES

- Melzack, R., and Casey, K.L. (1968). Sensory, motivational, and central control determinants of pain: a new conceptual model. In *The Skin Senses*, D. Kenshalo Springfield, ed. (C.C. Thomas), pp. 423–439.
- Vlaeyen, J.W.S., Crombez, G., and Linton, S.J. (2016). The fear-avoidance model of pain. *Pain* 157, 1588–1589. <https://doi.org/10.1097/j.pain.0000000000000574>.
- Kozłowska, K., Walker, P., McLean, L., and Carrive, P. (2015). Fear and the defense cascade: clinical implications and management. *Harv. Rev. Psychiatry* 23, 263–287. <https://doi.org/10.1097/HRP.0000000000000065>.
- Yilmaz, M., and Meister, M. (2013). Rapid innate defensive responses of mice to looming visual stimuli. *Curr. Biol.* 23, 2011–2015. <https://doi.org/10.1016/j.cub.2013.08.015>.
- Koutsikou, S., Apps, R., and Lumb, B.M. (2017). Top down control of spinal sensorimotor circuits essential for survival. *J. Physiol.* 595, 4151–4158. <https://doi.org/10.1113/JP273360>.
- Benarroch, E.E. (2008). Descending monoaminergic pain modulation: bidirectional control and clinical relevance. *Neurology* 71, 217–221. <https://doi.org/10.1212/01.wnl.0000318225.51122.63>.
- Lanius, R.A., Boyd, J.E., McKinnon, M.C., Nicholson, A.A., Frewen, P., Vermetten, E., Jetly, R., and Spiegel, D. (2018). A review of the neurobiological basis of trauma-related dissociation and its relation to cannabinoid- and opioid-mediated stress response: a transdiagnostic, translational approach. *Curr. Psychiatry Rep.* 20, 118. <https://doi.org/10.1007/s11920-018-0983-y>.
- Gross, C.T., and Canteras, N.S. (2012). The many paths to fear. *Nat. Rev. Neurosci.* 13, 651–658. <https://doi.org/10.1038/nrn3301>.
- Coghill, R.C. (2020). The distributed nociceptive system: a framework for understanding pain. *Trends Neurosci.* 43, 780–794. <https://doi.org/10.1016/j.tins.2020.07.004>.
- Davis, K.D., Flor, H., Greely, H.T., Iannetti, G.D., Mackey, S., Ploner, M., Pustilnik, A., Tracey, I., Treede, R.D., and Wager, T.D. (2017). Brain imaging tests for chronic pain: medical, legal and ethical issues and recommendations. *Nat. Rev. Neurol.* 13, 624–638. <https://doi.org/10.1038/nrneuro.2017.122>.
- Buckner, R.L., Krienen, F.M., and Yeo, B.T. (2013). Opportunities and limitations of intrinsic functional connectivity MRI. *Nat. Neurosci.* 16, 832–837. <https://doi.org/10.1038/nn.3423>.
- Lee, J.H., Durand, R., Gradinaru, V., Zhang, F., Goshen, I., Kim, D.S., Fenno, L.E., Ramakrishnan, C., and Deisseroth, K. (2010). Global and local fMRI signals driven by neurons defined optogenetically by type and wiring. *Nature* 465, 788–792. <https://doi.org/10.1038/nature09108>.
- Bliss, T.V., Collingridge, G.L., Kaang, B.K., and Zhuo, M. (2016). Synaptic plasticity in the anterior cingulate cortex in acute and chronic pain. *Nat. Rev. Neurosci.* 17, 485–496. <https://doi.org/10.1038/nrn.2016.68>.
- Zhao, M.G., Ko, S.W., Wu, L.J., Toyoda, H., Xu, H., Quan, J., Li, J., Jia, Y., Ren, M., Xu, Z.C., and Zhuo, M. (2006). Enhanced presynaptic neurotransmitter release in the anterior cingulate cortex of mice with chronic pain. *J. Neurosci.* 26, 8923–8930. <https://doi.org/10.1523/JNEUROSCI.2103-06.2006>.
- Xu, H., Wu, L.J., Wang, H., Zhang, X., Vadakkan, K.I., Kim, S.S., Steenland, H.W., and Zhuo, M. (2008). Presynaptic and postsynaptic amplifications of neuropathic pain in the anterior cingulate cortex. *J. Neurosci.* 28, 7445–7453. <https://doi.org/10.1523/JNEUROSCI.1812-08.2008>.
- Koga, K., Descalzi, G., Chen, T., Ko, H.G., Lu, J., Li, S., Son, J., Kim, T., Kwak, C., Haganir, R.L., et al. (2015). Coexistence of two forms of LTP in ACC provides a synaptic mechanism for the interactions between anxiety and chronic pain. *Neuron* 85, 377–389. <https://doi.org/10.1016/j.neuron.2014.12.021>.
- Calejesan, A.A., Kim, S.J., and Zhuo, M. (2000). Descending facilitatory modulation of a behavioral nociceptive response by stimulation in the adult rat anterior cingulate cortex. *Eur. J. Pain* 4, 83–96. <https://doi.org/10.1053/eujp.1999.0158>.
- Johansen, J.P., and Fields, H.L. (2004). Glutamatergic activation of anterior cingulate cortex produces an aversive teaching signal. *Nat. Neurosci.* 7, 398–403. <https://doi.org/10.1038/nn1207>.
- Tang, J., Ko, S., Ding, H.K., Qiu, C.S., Calejesan, A.A., and Zhuo, M. (2005). Pavlovian fear memory induced by activation in the anterior cingulate cortex. *Mol. Pain* 1, 6. <https://doi.org/10.1186/1744-8069-1-6>.
- Chen, T., Taniguchi, W., Chen, Q.Y., Tozaki-Saitoh, H., Song, Q., Liu, R.H., Koga, K., Matsuda, T., Kaito-Sugimura, Y., Wang, J., et al. (2018). Top-down descending facilitation of spinal sensory excitatory transmission from the anterior cingulate cortex. *Nat. Commun.* 9, 1886. <https://doi.org/10.1038/s41467-018-04309-2>.
- Ortiz, S., Latsko, M.S., Fouty, J.L., Dutta, S., Adkins, J.M., and Jasnow, A.M. (2019). Anterior cingulate cortex and ventral hippocampal inputs to the basolateral amygdala selectively control generalized fear. *J. Neurosci.* 39, 6526–6539. <https://doi.org/10.1523/JNEUROSCI.0810-19.2019>.
- Bian, X.L., Qin, C., Cai, C.Y., Zhou, Y., Tao, Y., Lin, Y.H., Wu, H.Y., Chang, L., Luo, C.X., and Zhu, D.Y. (2019). Anterior cingulate cortex to ventral hippocampus circuit mediates contextual fear generalization. *J. Neurosci.* 39, 5728–5739. <https://doi.org/10.1523/JNEUROSCI.2739-18.2019>.
- Steenland, H.W., Li, X.Y., and Zhuo, M. (2012). Predicting aversive events and terminating fear in the mouse anterior cingulate cortex during trace fear conditioning. *J. Neurosci.* 32, 1082–1095. <https://doi.org/10.1523/JNEUROSCI.5566-11.2012>.
- Han, C., O’Tuathaigh, C.M., van Trigt, L., Quinn, J.J., Fanselow, M.S., Mongeau, R., Koch, C., and Anderson. (2003). Trace but not delay fear conditioning requires attention and the anterior cingulate cortex. *Proc. Natl. Acad. Sci. USA* 100, 13087–13092.
- Schwartz, N., Temkin, P., Jurado, S., Lim, B.K., Heifets, B.D., Polepalli, J.S., and Malenka, R.C. (2014). Chronic pain. Decreased motivation during chronic pain requires long-term depression in the nucleus accumbens. *Science* 345, 535–542. <https://doi.org/10.1126/science.1253994>.
- Jin, Y., Meng, Q., Mei, L., Zhou, W., Zhu, X., Mao, Y., Xie, W., Zhang, X., Luo, M.H., Tao, W., et al. (2020). A somatosensory cortex input to the caudal dorsolateral striatum controls comorbid anxiety in persistent pain. *Pain* 161, 416–428. <https://doi.org/10.1097/j.pain.0000000000001724>.
- Li, N., Chen, S., Guo, Z.V., Chen, H., Huo, Y., Inagaki, H.K., Chen, G., Davis, C., Hansel, D., Guo, C., et al. (2019). Spatiotemporal constraints on optogenetic inactivation in cortical circuits. *eLife* 8, e48622. <https://doi.org/10.7554/eLife.48622>.
- Moon, H.S., Jiang, H., Vo, T.T., Jung, W.B., Vazquez, A.L., and Kim, S.G. (2021). Contribution of excitatory and inhibitory neuronal activity to BOLD fMRI. *Cereb. Cortex* 31, 4053–4067. <https://doi.org/10.1093/cercor/bhab068>.
- Jung, W.B., Jiang, H., Lee, S., and Kim, S.G. (2022). Dissection of brain-wide resting-state and functional somatosensory circuits by fMRI with optogenetic silencing. *Proc. Natl. Acad. Sci. USA* 119, <https://doi.org/10.1073/pnas.2113313119>.

30. You, T., Im, G.H., and Kim, S.G. (2021). Characterization of brain-wide somatosensory BOLD fMRI in mice under dexmedetomidine/isoflurane and ketamine/xylazine. *Sci. Rep.* *11*, 13110. <https://doi.org/10.1038/s41598-021-92582-5>.
31. Kim, S.G., and Ogawa, S. (2012). Biophysical and physiological origins of blood oxygenation level-dependent fMRI signals. *J. Cereb. Blood Flow Metab.* *32*, 1188–1206. <https://doi.org/10.1038/jcbfm.2012.23>.
32. Logothetis, N.K. (2008). What we can do and what we cannot do with fMRI. *Nature* *453*, 869–878. <https://doi.org/10.1038/nature06976>.
33. Petersen, C.C.H. (2019). Sensorimotor processing in the rodent barrel cortex. *Nat. Rev. Neurosci.* *20*, 533–546. <https://doi.org/10.1038/s41583-019-0200-y>.
34. Evans, D.A., Stempel, A.V., Vale, R., Rühle, S., Lefler, Y., and Branco, T. (2018). A synaptic threshold mechanism for computing escape decisions. *Nature* *558*, 590–594. <https://doi.org/10.1038/s41586-018-0244-6>.
35. Lischinsky, J.E., and Lin, D. (2019). Looming danger: unraveling the circuitry for predator threats. *Trends Neurosci.* *42*, 841–842. <https://doi.org/10.1016/j.tins.2019.10.004>.
36. Logothetis, N.K., Pauls, J., Augath, M., Trinath, T., and Oeltermann, A. (2001). Neurophysiological investigation of the basis of the fMRI signal. *Nature* *412*, 150–157. <https://doi.org/10.1038/35084005>.
37. Huang, J., Gadotti, V.M., Chen, L., Souza, I.A., Huang, S., Wang, D., Ramakrishnan, C., Deisseroth, K., Zhang, Z., and Zamponi, G.W. (2019). A neuronal circuit for activating descending modulation of neuropathic pain. *Nat. Neurosci.* *22*, 1659–1668. <https://doi.org/10.1038/s41593-019-0481-5>.
38. Yin, J.B., Liang, S.H., Li, F., Zhao, W.J., Bai, Y., Sun, Y., Wu, Z.Y., Ding, T., Sun, Y., Liu, H.X., et al. (2020). dmPFC-vIPAG projection neurons contribute to pain threshold maintenance and antianxiety behaviors. *J. Clin. Invest.* *130*, 6555–6570. <https://doi.org/10.1172/JCI127607>.
39. Drake, R.A., Steel, K.A., Apps, R., Lumb, B.M., and Pickering, A.E. (2021). Loss of cortical control over the descending pain modulatory system determines the development of the neuropathic pain state in rats. *eLife* *10*, e65156. <https://doi.org/10.7554/eLife.65156>.
40. Zhao, R., Zhou, H., Huang, L., Xie, Z., Wang, J., Gan, W.B., and Yang, G. (2018). Neuropathic pain causes pyramidal neuronal hyperactivity in the anterior cingulate cortex. *Front. Cell. Neurosci.* *12*, 107. <https://doi.org/10.3389/fncel.2018.00107>.
41. Büchel, C., Bornhoved, K., Quante, M., Glauche, V., Bromm, B., and Weiller, C. (2002). Dissociable neural responses related to pain intensity, stimulus intensity, and stimulus awareness within the anterior cingulate cortex: a parametric single-trial laser functional magnetic resonance imaging study. *J. Neurosci.* *22*, 970–976.
42. Zhou, H., Zhang, Q., Martinez, E., Dale, J., Hu, S., Zhang, E., Liu, K., Huang, D., Yang, G., Chen, Z., and Wang, J. (2018). Ketamine reduces aversion in rodent pain models by suppressing hyperactivity of the anterior cingulate cortex. *Nat. Commun.* *9*, 3751. <https://doi.org/10.1038/s41467-018-06295-x>.
43. Baliki, M.N., Chialvo, D.R., Geha, P.Y., Levy, R.M., Harden, R.N., Parrish, T.B., and Apkarian, A.V. (2006). Chronic pain and the emotional brain: specific brain activity associated with spontaneous fluctuations of intensity of chronic back pain. *J. Neurosci.* *26*, 12165–12173. <https://doi.org/10.1523/JNEUROSCI.3576-06.2006>.
44. Zhang, L., Zhang, Y., and Zhao, Z.Q. (2005). Anterior cingulate cortex contributes to the descending facilitatory modulation of pain via dorsal reticular nucleus. *Eur. J. Neurosci.* *22*, 1141–1148. <https://doi.org/10.1111/j.1460-9568.2005.04302.x>.
45. Zugaib, J., Coutinho, M.R., Ferreira, M.D., and Menescal-de-Oliveira, L. (2014). Glutamate/GABA balance in ACC modulates the nociceptive responses of vocalization: an expression of affective-motivational component of pain in guinea pigs. *Physiol. Behav.* *126*, 8–14. <https://doi.org/10.1016/j.physbeh.2013.12.004>.
46. Barthas, F., Sellmeijer, J., Hugel, S., Waltisperger, E., Barrot, M., and Yalcin, I. (2015). The anterior cingulate cortex is a critical hub for pain-induced depression. *Biol. Psychiatry* *77*, 236–245. <https://doi.org/10.1016/j.biopsych.2014.08.004>.
47. Kang, S.J., Kwak, C., Lee, J., Sim, S.E., Shim, J., Choi, T., Collingridge, G.L., Zhuo, M., and Kaang, B.K. (2015). Bidirectional modulation of hyperalgesia via the specific control of excitatory and inhibitory neuronal activity in the ACC. *Mol. Brain* *8*, 81. <https://doi.org/10.1186/s13041-015-0170-6>.
48. Elina, K.C., Moon, H.C., Islam, J., Kim, H.K., and Park, Y.S. (2021). The effect of optogenetic inhibition of the anterior cingulate cortex in neuropathic pain following sciatic nerve injury. *J. Mol. Neurosci.* *71*, 638–650. <https://doi.org/10.1007/s12031-020-01685-7>.
49. Wu, L.J., Toyoda, H., Zhao, M.G., Lee, Y.S., Tang, J., Ko, S.W., Jia, Y.H., Shum, F.W., Zerbini, C.V., Bu, G., et al. (2005). Upregulation of forebrain NMDA NR2B receptors contributes to behavioral sensitization after inflammation. *J. Neurosci.* *25*, 11107–11116. <https://doi.org/10.1523/JNEUROSCI.1678-05.2005>.
50. Wang, H., Xu, H., Wu, L.J., Kim, S.S., Chen, T., Koga, K., Descalzi, G., Gong, B., Vadakkan, K.I., Zhang, X., et al. (2011). Identification of an adenyl cyclase inhibitor for treating neuropathic and inflammatory pain. *Sci. Transl. Med.* *3*, 65ra3. <https://doi.org/10.1126/scitranslmed.3001269>.
51. Li, X.Y., Ko, H.G., Chen, T., Descalzi, G., Koga, K., Wang, H., Kim, S.S., Shang, Y., Kwak, C., Park, S.W., et al. (2010). Alleviating neuropathic pain hypersensitivity by inhibiting PKMzeta in the anterior cingulate cortex. *Science* *330*, 1400–1404. <https://doi.org/10.1126/science.1191792>.
52. de Lima, M.A.X., Baldo, M.V.C., Oliveira, F.A., and Canteras, N.S. (2022). The anterior cingulate cortex and its role in controlling contextual fear memory to predatory threats. *eLife* *11*, e67007. <https://doi.org/10.7554/eLife.67007>.
53. Descalzi, G., Li, X.Y., Chen, T., Mercaldo, V., Koga, K., and Zhuo, M. (2012). Rapid synaptic potentiation within the anterior cingulate cortex mediates trace fear learning. *Mol. Brain* *5*, 6. <https://doi.org/10.1186/1756-6606-5-6>.
54. Gilmartin, M.R., Balderston, N.L., and Helmstetter, F.J. (2014). Prefrontal cortical regulation of fear learning. *Trends Neurosci.* *37*, 455–464. <https://doi.org/10.1016/j.tins.2014.05.004>.
55. Senapati, A.K., Lagraize, S.C., Huntington, P.J., Wilson, H.D., Fuchs, P.N., and Peng, Y.B. (2005). Electrical stimulation of the anterior cingulate cortex reduces responses of rat dorsal horn neurons to mechanical stimuli. *J. Neurophysiol.* *94*, 845–851. <https://doi.org/10.1152/jn.00040.2005>.
56. Fillinger, C., Yalcin, I., Barrot, M., and Veinante, P. (2018). Efferents of anterior cingulate areas 24a and 24b and midcingulate areas 24a' and 24b. *Brain Struct. Funct.* *223*, 1747–1778. <https://doi.org/10.1007/s00429-017-1585-x>.
57. Beitz, A.J. (1989). Possible origin of glutamatergic projections to the midbrain periaqueductal gray and deep layer of the superior colliculus of the rat. *Brain Res. Bull.* *23*, 25–35. [https://doi.org/10.1016/0361-9230\(89\)90159-7](https://doi.org/10.1016/0361-9230(89)90159-7).
58. Coutinho, M.R., and Menescal-de-Oliveira, L. (2010). Role of homocysteic acid in the guinea pig (*Cavia porcellus*) anterior cingulate cortex in tonic immobility and the influence of NMDA receptors on the dorsal PAG. *Behav. Brain Res.* *208*, 237–242. <https://doi.org/10.1016/j.bbr.2009.11.047>.
59. Jhang, J., Lee, H., Kang, M.S., Lee, H.S., Park, H., and Han, J.H. (2018). Anterior cingulate cortex and its input to the basolateral amygdala control innate fear response. *Nat. Commun.* *9*, 2744. <https://doi.org/10.1038/s41467-018-05090-y>.
60. Wang, G.Q., Cen, C., Li, C., Cao, S., Wang, N., Zhou, Z., Liu, X.M., Xu, Y., Tian, N.X., Zhang, Y., et al. (2015). Deactivation of excitatory neurons in the prelimbic cortex via Cdk5 promotes pain sensation and anxiety. *Nat. Commun.* *6*, 7660. <https://doi.org/10.1038/ncomms8660>.
61. Zhou, H., Martinez, E., Lin, H.H., Yang, R., Dale, J.A., Liu, K., Huang, D., and Wang, J. (2018). Inhibition of the prefrontal projection to the nucleus

- accumbens enhances pain sensitivity and affect. *Front. Cell. Neurosci.* 12, 240. <https://doi.org/10.3389/fncel.2018.00240>.
62. Kragel, P.A., Kano, M., Van Oudenhove, L., Ly, H.G., Dupont, P., Rubio, A., Delon-Martin, C., Bonaz, B.L., Manuck, S.B., Gianaros, P.J., et al. (2018). Generalizable representations of pain, cognitive control, and negative emotion in medial frontal cortex. *Nat. Neurosci.* 21, 283–289. <https://doi.org/10.1038/s41593-017-0051-7>.
63. Laubach, M., Amarante, L.M., Swanson, K., and White, S.R. (2018). What, if anything, is rodent prefrontal cortex? *eNeuro* 5, 0315–18.2018. <https://doi.org/10.1523/ENEURO.0315-18.2018>.
64. Carlén, M. (2017). What constitutes the prefrontal cortex? *Science* 358, 478–482. <https://doi.org/10.1126/science.aan8868>.
65. Mobbs, D., Marchant, J.L., Hassabis, D., Seymour, B., Tan, G., Gray, M., Petrovic, P., Dolan, R.J., and Frith, C.D. (2009). From threat to fear: the neural organization of defensive fear systems in humans. *J. Neurosci.* 29, 12236–12243. <https://doi.org/10.1523/JNEUROSCI.2378-09.2009>.
66. Roy, M., Shohamy, D., Daw, N., Jepma, M., Wimmer, G.E., and Wager, T.D. (2014). Representation of aversive prediction errors in the human periaqueductal gray. *Nat. Neurosci.* 17, 1607–1612. <https://doi.org/10.1038/nn.3832>.
67. Petrovic, P., Petersson, K.M., Ghatan, P.H., Stone-Elander, S., and Ingvar, M. (2000). Pain-related cerebral activation is altered by a distracting cognitive task. *Pain* 85, 19–30. [https://doi.org/10.1016/s0304-3959\(99\)00232-8](https://doi.org/10.1016/s0304-3959(99)00232-8).
68. Valet, M., Sprenger, T., Boecker, H., Willoch, F., Rummeny, E., Conrad, B., Erhard, P., and Tolle, T.R. (2004). Distraction modulates connectivity of the cingulo-frontal cortex and the midbrain during pain—an fMRI analysis. *Pain* 109, 399–408. <https://doi.org/10.1016/j.pain.2004.02.033>.
69. Oliva, V., Gregory, R., Davies, W.E., Harrison, L., Moran, R., Pickering, A.E., and Brooks, J.C.W. (2021). Parallel cortical-brainstem pathways to attentional analgesia. *Neuroimage* 226, 117548. <https://doi.org/10.1016/j.neuroimage.2020.117548>.
70. Bryden, D.W., Johnson, E.E., Tobia, S.C., Kashtelyan, V., and Roesch, M.R. (2011). Attention for learning signals in anterior cingulate cortex. *J. Neurosci.* 31, 18266–18274. <https://doi.org/10.1523/JNEUROSCI.4715-11.2011>.
71. Hayden, B.Y., Heilbronner, S.R., Pearson, J.M., and Platt, M.L. (2011). Surprise signals in anterior cingulate cortex: neuronal encoding of unsigned reward prediction errors driving adjustment in behavior. *J. Neurosci.* 31, 4178–4187. <https://doi.org/10.1523/JNEUROSCI.4652-10.2011>.
72. Schneider, K.N., Sciarillo, X.A., Nudelman, J.L., Cheer, J.F., and Roesch, M.R. (2020). Anterior cingulate cortex signals attention in a social paradigm that manipulates reward and shock. *Curr. Biol.* 30, 3724–3735.e2. <https://doi.org/10.1016/j.cub.2020.07.039>.
73. Shima, K., and Tanji, J. (1998). Role of cingulate motor area cells in voluntary movement selection based on reward. *Science* 282, 1335–1338. <https://doi.org/10.1126/science.282.5392.1335>.
74. Paus, T. (2001). Primate anterior cingulate cortex: where motor control, drive and cognition interface. *Nat. Rev. Neurosci.* 2, 417–424. <https://doi.org/10.1038/35077500>.
75. Williams, Z.M., Bush, G., Rauch, S.L., Cosgrove, G.R., and Eskandar, E.N. (2004). Human anterior cingulate neurons and the integration of monetary reward with motor responses. *Nat. Neurosci.* 7, 1370–1375. <https://doi.org/10.1038/nn1354>.
76. Wei, P., Liu, N., Zhang, Z., Liu, X., Tang, Y., He, X., Wu, B., Zhou, Z., Liu, Y., Li, J., et al. (2015). Processing of visually evoked innate fear by a non-canonical thalamic pathway. *Nat. Commun.* 6, 6756. <https://doi.org/10.1038/ncomms7756>.
77. Zhou, Z., Liu, X., Chen, S., Zhang, Z., Liu, Y., Montardy, Q., Tang, Y., Wei, P., Liu, N., Li, L., et al. (2019). A VTA GABAergic neural circuit mediates visually evoked innate defensive responses. *Neuron* 103, 473–488.e6. <https://doi.org/10.1016/j.neuron.2019.05.027>.
78. Huda, R., Sipe, G.O., Breton-Provencher, V., Cruz, K.G., Pho, G.N., Adam, E., Gunter, L.M., Sullins, A., Wickersham, I.R., and Sur, M. (2020). Distinct prefrontal top-down circuits differentially modulate sensorimotor behavior. *Nat. Commun.* 11, 6007. <https://doi.org/10.1038/s41467-020-19772-z>.
79. Pan, W.X., Mao, T., and Dudman, J.T. (2010). Inputs to the dorsal striatum of the mouse reflect the parallel circuit architecture of the forebrain. *Front. Neuroanat.* 4, 147. <https://doi.org/10.3389/fnana.2010.00147>.
80. Bosch-Bouju, C., Hyland, B.I., and Parr-Brownlie, L.C. (2013). Motor thalamus integration of cortical, cerebellar and basal ganglia information: implications for normal and parkinsonian conditions. *Front. Comput. Neurosci.* 7, 163. <https://doi.org/10.3389/fncom.2013.00163>.
81. Mallet, N., Delgado, L., Chazalon, M., Miguez, C., and Baufreton, J. (2019). Cellular and synaptic dysfunctions in Parkinson's disease: stepping out of the striatum. *Cells* 8, 1005. <https://doi.org/10.3390/cells8091005>.
82. Alloway, K.D., Smith, J.B., and Beauchemin, K.J. (2010). Quantitative analysis of the bilateral brainstem projections from the whisker and forepaw regions in rat primary motor cortex. *J. Comp. Neurol.* 518, 4546–4566. <https://doi.org/10.1002/cne.22477>.
83. Pagano, R.L., Fonoff, E.T., Dale, C.S., Ballester, G., Teixeira, M.J., and Britto, L.R.G. (2012). Motor cortex stimulation inhibits thalamic sensory neurons and enhances activity of PAG neurons: possible pathways for antinociception. *Pain* 153, 2359–2369. <https://doi.org/10.1016/j.pain.2012.08.002>.
84. Magno, L.A.V., Tenza-Ferrer, H., Colodetti, M., Aguiar, M.F.G., Rodrigues, A.P.C., da Silva, R.S., Silva, J.D.P., Nicolau, N.F., Rosa, D.V.F., Birbrair, A., et al. (2019). Optogenetic stimulation of the M2 cortex reverts motor dysfunction in a mouse model of Parkinson's disease. *J. Neurosci.* 39, 3234–3248. <https://doi.org/10.1523/JNEUROSCI.2277-18.2019>.
85. Holroyd, C.B., and Yeung, N. (2012). Motivation of extended behaviors by anterior cingulate cortex. *Trends Cogn. Sci.* 16, 122–128. <https://doi.org/10.1016/j.tics.2011.12.008>.
86. Nass, S.R., Hahn, Y.K., McLane, V.D., Varshneya, N.B., Damaj, M.I., Knapp, P.E., and Hauser, K.F. (2020). Chronic HIV-1 Tat exposure alters anterior cingulate cortico-basal ganglia-thalamocortical synaptic circuitry, associated behavioral control, and immune regulation in male mice. *Brain Behav Immun Health* 5, 100077. <https://doi.org/10.1016/j.bbih.2020.100077>.
87. Woo, C.W., Roy, M., Buhle, J.T., and Wager, T.D. (2015). Distinct brain systems mediate the effects of nociceptive input and self-regulation on pain. *PLoS Biol.* 13, e1002036. <https://doi.org/10.1371/journal.pbio.1002036>.
88. Smith, M.L., Asada, N., and Malenka, R.C. (2021). Anterior cingulate inputs to nucleus accumbens control the social transfer of pain and analgesia. *Science* 371, 153–159. <https://doi.org/10.1126/science.abe3040>.
89. Deyama, S., Nakagawa, T., Kaneko, S., Uehara, T., and Minami, M. (2007). Involvement of the bed nucleus of the stria terminalis in the negative affective component of visceral and somatic pain in rats. *Behav. Brain Res.* 176, 367–371. <https://doi.org/10.1016/j.bbr.2006.10.021>.
90. Hulsman, A.M., Terburg, D., Roelofs, K., and Klumpers, F. (2021). Roles of the bed nucleus of the stria terminalis and amygdala in fear reactions. *Handb. Clin. Neurol.* 179, 419–432. <https://doi.org/10.1016/B978-0-12-819975-6.00027-3>.
91. Nogueira, R., Abolafia, J.M., Drugowitsch, J., Balaguer-Ballester, E., Sanchez-Vives, M.V., and Moreno-Bote, R. (2017). Lateral orbitofrontal cortex anticipates choices and integrates prior with current information. *Nat. Commun.* 8, 14823. <https://doi.org/10.1038/ncomms14823>.
92. Ong, W.Y., Stohler, C.S., and Herr, D.R. (2019). Role of the prefrontal cortex in pain processing. *Mol. Neurobiol.* 56, 1137–1166. <https://doi.org/10.1007/s12035-018-1130-9>.
93. Huang, J., Zhang, Z., Gambeta, E., Chen, L., and Zamponi, G.W. (2021). An orbitofrontal cortex to midbrain projection modulates hypersensitivity

- after peripheral nerve injury. *Cell Rep.* 35, 109033. <https://doi.org/10.1016/j.celrep.2021.109033>.
94. de Lima, M.A., Baldo, M.V., and Canteras, N.S. (2017). A role for the anteromedial thalamic nucleus in the acquisition of contextual fear memory to predatory threats. *Brain Struct. Funct.* 222, 113–129. <https://doi.org/10.1007/s00429-016-1204-2>.
95. Rangel, M.J., Jr., Baldo, M.V.C., and Canteras, N.S. (2018). Influence of the anteromedial thalamus on social defeat-associated contextual fear memory. *Behav. Brain Res.* 339, 269–277. <https://doi.org/10.1016/j.bbr.2017.10.038>.
96. Nelson, A.J.D. (2021). The anterior thalamic nuclei and cognition: a role beyond space? *Neurosci. Biobehav. Rev.* 126, 1–11. <https://doi.org/10.1016/j.neubiorev.2021.02.047>.
97. Jung, W.B., Im, G.H., Jiang, H., and Kim, S.G. (2021). Early fMRI responses to somatosensory and optogenetic stimulation reflect neural information flow. *Proc. Natl. Acad. Sci. USA* 118, <https://doi.org/10.1073/pnas.2023265118>.
98. Cimadevilla, J.M., Wesierska, M., Fenton, A.A., and Bures, J. (2001). Inactivating one hippocampus impairs avoidance of a stable room-defined place during dissociation of arena cues from room cues by rotation of the arena. *Proc. Natl. Acad. Sci. USA* 98, 3531–3536. <https://doi.org/10.1073/pnas.051628398>.
99. Bullmore, E., and Sporns, O. (2009). Complex brain networks: graph theoretical analysis of structural and functional systems. *Nat. Rev. Neurosci.* 10, 186–198. <https://doi.org/10.1038/nrn2575>.
100. Zalesky, A., Fornito, A., and Bullmore, E.T. (2010). Network-based statistic: identifying differences in brain networks. *Neuroimage* 53, 1197–1207. <https://doi.org/10.1016/j.neuroimage.2010.06.041>.

## STAR★METHODS

### KEY RESOURCES TABLE

REAGENT or RESOURCE	SOURCE	IDENTIFIER
<b>Bacterial and virus strains</b>		
AAV5-CaMKIIa-hChr2(H134R)-eTFP	Addgene	Cat#26969-AAV5;RRID:Addgene_26969
AAV5-CaMKIIa-eArch3.0-eYFP	UNC Vector	N/A
AAV5-CaMKIIa-eYFP	UNC Vector	N/A
AAV5-CaMKIIa-mCherry	Addgene	Cat#114469-AAV5
<b>Chemicals, peptides, and recombinant proteins</b>		
Capsaicin	Sigma-Aldrich	Cat#M2028
Freund's Adjuvant, Complete (CFA)	Sigma-Aldrich	Cat#F5881
<b>Experimental models: Organisms/strains</b>		
Mouse:C57BL/6J	OrientBio (South Korea)	N/A
Mouse: VGAT-ChR2-eYFP (B6.Cg-Tg (Slc32a1-COP4*H134R/eYFP 8Gfng/J)	The Jackson Laboratory	RRID:IMSR_JAX:014548
<b>Software and algorithms</b>		
MATLAB R2020b	MathWorks	<a href="https://www.mathworks.com">https://www.mathworks.com</a> ; RRID: SCR_001622
Brain Connectivity Toolbox	MATLAB Brain Connectivity Toolbox	<a href="https://sites.google.com/site/bctnet/">https://sites.google.com/site/bctnet/</a> ; PRID:SCR_004841
FSL	Analysis Group, FMRIB, Oxford, UK	<a href="https://fsl.fmrib.ox.ac.uk/fsl/fslwiki/">https://fsl.fmrib.ox.ac.uk/fsl/fslwiki/</a> ; RRID: SCR_002823
AFNI	SSCC at NIMH	<a href="https://afni.nimh.nih.gov/">https://afni.nimh.nih.gov/</a> ; RRID: SCR_005927
SPM12	Wellcome Department of Cognitive Neurology, London, UK	<a href="https://www.fil.ion.ucl.ac.uk/spm/">https://www.fil.ion.ucl.ac.uk/spm/</a> ; RRID: SCR_002823
GraphPad 9.0	Prism	<a href="http://www.graphpad.com">www.graphpad.com</a> ; RRID:SCR_002798
EthoVision XT	Noldus	<a href="https://www.noldus.com/ethovision-xt">https://www.noldus.com/ethovision-xt</a> ; PRID:SCR_000441

### RESOURCE AVAILABILITY

#### Lead contact

Further information and requests for resources and reagents should be directed to and will be fulfilled by the lead contact, Seong-Gi Kim ([seonggikim@skku.edu](mailto:seonggikim@skku.edu)).

#### Materials availability

This study did not generate new unique reagents.

#### Data and code availability

- All data reported in this paper will be shared by the [lead contact](#) upon request.
- This paper does not report original code.
- Any additional information required to reanalyze the data reported in this paper is available from the [lead contact](#) upon request.

### EXPERIMENTAL MODEL AND SUBJECT DETAILS

#### Animals

All experimental procedures were reviewed and approved by the Institutional Animal Care and Use Committee (IACUC) at Sungkyunkwan University and followed relevant guidelines and regulations confirmed by IACUC. Adult male C57BL/6 mice ( $n = 42$ ) aged 7 to 10 weeks were purchased from Orient Bio (Seongnam, Korea), and VGAT-ChR2-eYFP (B6.Cg-Tg (Slc32a1-COP4\*H134R/eYFP 8Gfng/J) mice were bred in-house from breeding pairs obtained from Jackson Laboratory (Bar Harbor, ME, USA). Both male ( $n=5$ ) and female ( $n = 15$ ) VGAT-ChR2-eYFP mice and VGAT-ChR2-eYFP negative female littermates ( $n = 4$ ) were used. The exact number of mice for each experiment can be found in the figure legends. Mice were housed independently in ventilated cages post-surgery in a temperature/humidity-controlled facility and maintained with standard lab chow and water ad libitum under a 12-hour dark-light cycle. Behavior and fMRI experiments were conducted

three-four weeks post-surgery. Behavior differences between genders were not observed and thus both genders were grouped for analysis.

## METHOD DETAILS

### Stereotaxic surgery

The adeno-associated viruses (AAVs) were purchased from Addgene or UNC Vector Core; AAV5-CaMKIIa-hChR2(H134R)-eYFP (Addgene), AAV5-CaMKIIa-eArch3.0-eYFP (UNC Vector), AAV5-CaMKIIa-eYFP (UNC Vector), AAV5-CaMKIIa-mCherry (Addgene). Mice were initially inducted with inhaled isoflurane (Hana, Korea) and then anesthetized by intraperitoneal (IP) injection of ketamine (Yuhan, Korea) and xylazine (Rompun<sup>®</sup>, Bayer, Korea) mixture (100 mg/kg and 10 mg/kg) before fixing onto a stereotaxic frame. To maintain the anesthetic conditions throughout surgery duration, isoflurane (0.5-1.0 %) in oxygen and air gases (1:4 ratio) was used, based on physiological signal changes. To alleviate pain and inflammation, lidocaine (Daihan, Korea) was subcutaneously injected into the scalp, and Metacam (5 mg/kg, meloxicam, Boehringer Ingelheim, Korea) was injected subcutaneously into the loose skin over the neck. Male C57BL6 mice were used for viral infection into left side of ACC (anteroposterior [AP], 1.0 mm relative to bregma; mediolateral [ML], 0.3 mm; dorsoventral [DV], 1 mm relative to surface) or left side of PrL ([AP], 2.5 mm relative to bregma; [ML], 0.3 mm; [DV], 1 mm relative to surface). A glass capillary was connected to the injection pump (Nanoliter 2010, World Precision Instruments) and a total 1  $\mu$ l of viral suspension was filled. After virus injection, optic fiber (105  $\mu$ m inner core diameter, NA = 0.22, 2 mm, Thorlabs, USA) for optogenetic modulation was immediately implanted at the same [AP] and [ML] coordinates, except for 0.8 mm [DV] relative to surface. For the optogenetic modulation of ACC input to PAG, the optic fiber (100  $\mu$ m inner core diameter, NA = 0.22, 3.5mm, Doric Lenses Inc, Canada) was inserted into left side of PAG ([AP], -4.0 mm relative to bregma; [ML], 0.5 mm; [DV], 1.9 mm relative to the surface), following virus injection into the ACC. For VGAT-ChR2 group, only the optic fiber was implanted without virus injection. We used bio-compatible silicon elastomer (Kwik-Sil, World Precision Instruments, Sarasota, FL, USA) to seal the fiber implantation site and dental cement (SB, Sun-Medical Co., Shiga, Japan) to fix the optic fiber onto the skull. Behavior or ofMRI experiments were conducted at least 3-4 weeks after virus injection/fiber implantation.

### Optogenetics

The location of optic fiber was confirmed by an anatomical image using MRI. For the behavior test, the implanted optic fiber was connected to a fiber-optic cable (Doric Lenses Inc, Canada) coupled to 473 nm, 532 nm, or 566 nm diode-pumped solid state laser (Changchun New Industries Optoelectronics Tech. Co., Ltd, Changchun, China). The constant output power was calibrated to be 3-5 mW at the tip of the optic fiber, as measured by a power meter (PM100D, Thorlabs, USA). The experimental procedure for ofMRI was previously described in detail.<sup>97</sup> The implanted optic fiber was connected to Low Profile Patch Cord Adapter (LPPA) to modify the direction path of a patch cord without bending the fiber cable. 437 nm, 532 nm, or 566 nm diode-pumped solid state laser (Changchun New Industries Optoelectronics Tech. Co., Ltd, Changchun, China) was used, and the constant output power was calibrated to be 3 mW at the tip of the optic fiber. The intensity of output power was adjusted according to the BOLD response. Given our previous research,<sup>28,29</sup> the light stimulus (437 nm) was delivered with 20 Hz/10ms parameters to silence excitatory pyramidal neuron with VGAT-ChR2 mice. 532 nm (for behavior test) and 566 nm (for ofMRI) light was given continuously to silence excitatory pyramidal neuron using AAV5-CaMKIIa-eArch3.0-eYFP.

### Behavior tests

#### Thermal pain test (Hargreaves test)

To assess thermal-evoked pain, paw withdrawal latency was measured using the Hargreaves method (IITC Life Science Plantar Test, Victory Blvd Woodland Hills, CA, USA). Before the test, mice were habituated in an acrylic observation chamber (size ranges 10 x 10 x 15 cm<sup>3</sup>) on a glass plate. The infrared stimulation (48-50% or 80% intensity) was applied to the hind paw. Paw withdrawal latency was measured 4 to 5 times by an observer blinded to the treatment and then averaged, which was represented by thermal pain threshold.

#### Pain model

Before the induction of the pain model, the baseline of thermal pain threshold was measured. The induction of capsaicin/CFA-evoked pain hypersensitivity was confirmed by the decrease in thermal pain threshold compared to baseline or contralateral paw. For the capsaicin-induced acute pain model, capsaicin (Sigma, USA) was dissolved in DMSO, and 20  $\mu$ l of capsaicin (1  $\mu$ g, diluted in 0.9% saline) was injected into the plantar surface of the right hind paw. The time mice spent licking was measured during 10 minutes by an observer who was blinded to the genotype of mice. The thermal pain test was performed 20 minutes after capsaicin injection. For the CFA-induced chronic pain model, 20  $\mu$ l of undiluted CFA (Sigma, USA) was injected twice into the plantar surface of the right hind paw. The thermal pain test was performed 3 or 4 days after the first injection of CFA (before the second injection of CFA). Subsequently, the mice received a second injection of CFA 7 days after the first and the thermal pain test was performed once more.

#### Open field test

To assay locomotor activity and anxiety, the duration in the center or border zone and the speed of movement were measured by automated analysis software (EthoVision). The sound insulated behavioral room was illuminated by indirect dim lighting. Single mice were placed in the center of an acrylic apparatus (size ranges 50 x 50 x 38 cm<sup>3</sup>) consisting of the center zone (24 x 24 cm<sup>2</sup>) and the border zone, and then were allowed to explore freely. Optogenetic stimulations (473nm, 3~5mW, 20Hz, 10ms) were given over one minute with one-minute intervals between each. The ON-OFF period was repeated 3 times each. To quantify the anxiety

behavior, we calculated the speed of movement and the duration in the center zone or border zone. The effect of optogenetic stimulation was defined as the differences between ON and OFF.

#### **Fox urine-induced innate fear test**

Before the test, mice were habituated for 2 minutes in an acrylic apparatus (size ranges 35 x 25 x 23 cm<sup>3</sup>). Mice were exposed to fox urine in an inescapable environment consisting of zone1 (12 x 25 cm<sup>2</sup>) close to fox urine and zone2 (12 x 25 cm<sup>2</sup>) away from fox urine. Three sheets of KimWipes laboratory tissue were stacked, folded in half, and fixed in zone1. 2 ml of fox urine were applied. Optogenetic stimulation (473 nm, 3~5 mW, 20 Hz, 10 ms) was given over one minute with an interval of one minute between consecutive trials. The ON-OFF period was repeated 3 times each. Using automated analysis software (EthoVision), the duration in zone1 or zone2 and the speed of movement were measured. The effect of optogenetic stimulation was defined as the differences between ON and OFF.

#### **Active place avoidance task**

To evaluate the active avoidance behavior, we tested mice using APAT.<sup>98</sup> A custom-built rotating circular maze (radius: 17 cm) with transparent acrylic walls (height: 25 cm) and floor consisting of a metal grill (3.4 mm diameter bars with 1 cm spacing) was used for APAT training. The apparatus was placed in a well-lit isolation booth, which had distinct black-and-white visual patterns on four walls (vertical stripes, square grids, diagonal stripes, and polka dots). The rotation speed of the maze was given in rotations per minute (RPM). The position of the animal during the task was analyzed instantly with video tracking software (EthoVision). One to three days before the test, mice were habituated for 30 minutes inside the apparatus without any shocks or rotation. APAT training was conducted over two days following the habituation session. On day 1, mice underwent two sessions with different maze rotation speeds (3 RPM then 2 RPM) with an inter-session interval of two hours. In these sessions, whenever mice entered a pre-defined shock zone spanning one-sixth of the maze, the mice received a footshock (0.2 mA, 60 Hz) for 500ms. If the mice failed to exit the shock zone, additional footshocks were given every 1.5 seconds. On day 2, the same set of sessions were conducted with an addition of optogenetic stimulation. In each session, optogenetic stimulations (473 nm, 3~5 mW, 20 Hz, 10 ms) was given in an alternating pattern over five minutes with an interval of five minutes. To quantify the active avoidance behavior, we calculated the number of entries into the shock zone and mean angular distance from the shock zone for each of 5 min time bins. The effect of optogenetic stimulation was defined as the differences in angular distance between time bins when the first optogenetic stimulation was turned on (ON1) and the first 5 min bin when the laser was turned off (OFF1). Additionally, we used the differences in angular distance between the first two time bins (OFF1 and OFF2) with no optogenetic stimulation as a baseline.

## **MRI**

#### **Animal preparation**

All MRI experiments were performed on a 15.2T MRI scanner with an actively shielded 6-cm diameter gradient (Bruker BioSpec, Billerica, MA, USA) and a 15 mm ID surface coil for radiofrequency (RF) transmission/reception. BOLD fMRI was conducted on CFA (n = 8), naïve (n = 9), and ACC<sup>CaMKII</sup> (n = 7) group of mice under self-breathing IV continuous infusion dexmedetomidine/isoflurane (0.05 mg/kg/hr/0.3%) anesthesia described in detail previously.<sup>30</sup> Mice were induced with 2-4 % isoflurane during which the tail vein was cannulated for IV infusion of dexmedetomidine (Precedex, Hospira, NC, USA). Next, mice were secured to a custom-made MR cradle via ear and bite bar. The cradle was transferred to the magnet and connected to a small animal ventilator (Model 1030, Small Animal Instrument Inc., Stony Brook, USA). A bolus of 0.05 mg/kg dexmedetomidine was given after MR preparation followed by discontinuation of isoflurane. Infusion of dexmedetomidine at (0.05 mg/kg/hr) was started 10 min post bolus. Isoflurane was continued at 0.3% ~30 min post dexmedetomidine bolus. During the experiments, heart rate and motion-sensitive respiratory signals were continuously monitored (PhysioSuite, Kent Scientific Corp.) along with body temperature of the animals being maintained at 37 ± 0.5 °C with a warm-water heating system and a rectal thermometer.

#### **Data acquisition**

Data were acquired with Paravision 6.0.1 software. Image acquisition started after placing the mouse brain at the isocenter of the magnet and correcting for field inhomogeneity via the MAPSHIM protocol. Anatomical images were acquired using fast low angle shot (FLASH) sequence with the following parameters: TR/TE = 3000/45 ms, matrix size = 120 x 58, field of view (FOV) = 15.80 x 7.65 mm<sup>2</sup>, and 20 0.5-mm-thick slices. Functional images were acquired using gradient-echo single-shot echo planar imaging (EPI) with the following parameters: TR/TE = 1000/11.5 ms, matrix size = 120 x 58, FOV = 15.84 x 7.65 mm<sup>2</sup> (0.13 x 0.13 mm<sup>2</sup> in-plane resolution), 20 0.5-mm-thick slices, and 50° flip angle. To ensure best group alignment, the 6<sup>th</sup> slice was matched to the individual mouse's anterior commissure.

Functional scans were conducted in a block design of 60s baseline – 20s stimulation – 60s interstimulus interval – 20s stimulation – 60s recovery. The same optogenetic parameters used for behavior were used. In the naïve group of mice, a further whisker-pad (WP) stimulation was conducted in which the right whisker-pad was electrically stimulated with electrodes placed on the pad at 0.4mA, 4Hz.<sup>30</sup> Simultaneous WP and optogenetic stimulation (WPOG) were also conducted on the same group of mice.

#### **fMRI data pre-processing**

BOLD fMRI data were processed as previously described using AFNI, FSL, and SPM12.<sup>30</sup> Images were scaled 10x, despiked (AFNI, 3dDespike), motion-corrected (AFNI, 3dvolreg), and slice-time corrected (AFNI, 3dTshift). EPI images were then temporally averaged (fsl, fslmaths -Tmean) and skull stripped (fsl, bet) to create an EPI template for registration. Anatomical images were skull stripped (fsl, bet) and co-registered to the EPI template (SPM12). Linear affine parameters and nonlinear regularizations were calculated between the skull-stripped co-registered anatomical image and Allen Mouse Brain Common Coordinate Framework v3 (CCFv3) template, after which the deformations were applied to the functional images with SPM12's Normalize function.

### Viral tracing

Mice were sacrificed after behavior and ofMRI experiments were completed. Mice received a lethal dose of pentobarbital (> 60 mg/kg) and were perfused with 0.9% saline followed by 4% paraformaldehyde (PFA). The whole brain was post-fixed by 4% PFA, cryopreserved in 30% sucrose, and embedded in OCT compound. The frozen specimen was transversely sectioned into 40  $\mu\text{m}$  with a cryotome. Sections were mounted on a slide glass and nuclear staining was performed with DAPI solution (1:10000, sigma). Fluorescence images were obtained using a fluorescence microscope (Leica, Germany).

### Region of interest abbreviations

Abbreviations for all ROIs are the following: ACCd/v anterior cingulate cortex dorsal/ventral, Ald dorsal agranular insula, AM anteromedial thalamus, APN anterior pretectal nuclei, AV anteroventral thalamus, BNST bed nucleus of striata terminalis, CA1 hippocampus CA1 subfield, dl/IPAG dorsal-lateral lateral periaqueductal gray, DLS dorsolateral striatum, dmPAG dorsomedial PAG, GPe globus pallidus externa, IL infralimbic, LD lateral dorsal thalamus, LP lateral posterior thalamus, M1hl primary motor hindlimb region, M1wf primary motor whisker/forepaw region, M2 secondary motor cortex, MD mediodorsal thalamus, MRN midbrain reticular nucleus, OFCI lateral orbitofrontal cortex, PF parafascicular nucleus, PrL prelimbic cortex, PO posterior thalamus, PPCa posterior parietal cortex, RE nucleus reuniens, RSCd/v retrosplenial cortex dorsal/ventral, S1BF/FL/HL primary somatosensory barrel/forelimb/hindlimb, S2 secondary somatosensory, SCm motor superior colliculus, SN substantia nigra, SUB subiculum, V2al secondary anterolateral visual cortex, VAL ventral anterolateral thalamus, vlPAG ventral lateral PAG, VM ventromedial thalamus, VP ventral posterior thalamus, ZI zona incerta.

Abbreviations in anatomical tracing data follow: CM central medial thalamus, CL central lateral thalamus, cp cerebral peduncle, CPu caudate putamen, Ect ectorhinal cortex, ic internal capsule, PRh perirhinal cortex, PRN pontine reticular nucleus, Rt reticular thalamus, VA ventral anterior thalamus, VL ventral lateral thalamus, VPL ventral posterolateral thalamus, VPM ventral posteromedial thalamus

### QUANTIFICATION AND STATISTICAL ANALYSIS

Statistical details for every experiment are provided in the figure legends with “n” representing the number of animals per group. Group differences with  $p < 0.05$  were considered significant (\* $p < 0.05$ , \*\* $p < 0.01$ , \*\*\* $p < 0.001$ , \*\*\*\* $p < 0.0001$ ).

### Behavior analysis

Statistical analysis was performed using GraphPad Prism (GraphPad Software, USA). For comparison between two groups, statistical analyses were carried out using paired t-test or unpaired t-test (two-tailed) as appropriate. For multiple comparisons, data were analyzed using one-way ANOVA, repeated measures one-way ANOVA, or two-way ANOVA followed by Bonferroni test as appropriate. Data are presented as mean  $\pm$  SEM.

### GLM statistical mapping

Group BOLD response maps were generated by general linear model (GLM) by deconvolving the registered images with a design matrix containing a linear detrend and our previously designed dexmedetomidine hemodynamic response function convolved with the stimulation blocks as regressors (AFNI, 3dDeconvolve). Unpaired (CFA vs naïve), paired (WP vs WPOG), or one sample ( $\text{ACC}^{\text{CaMKII}}$ ) t-test was used to produce group response maps (AFNI, 3dttest++). The resultant maps were smoothed 2x the voxel size and cluster corrected by finding first-nearest neighbor clusters that pass the threshold of  $P < 0.005$  uncorrected and correcting them with a family-wise error correction to  $P < 0.05$  unless otherwise stated (AFNI, 3dClustsim).

### BOLD quantification

The registered functional images were normalized to the baseline to calculate percent signal change. Anatomical region of interests (ROI) based on the CCFv3 was used to extract the signal from each region. Areas such as dmPAG, dl/IPAG, and vlPAG did not have a segmented atlas and thus a square 9 voxel ROI was drawn in each respective area within the PAG. For signal quantification, the extracted time series were temporally smoothed with a 6-second window to remove sharp outliers and area-under-curve (AUC) was calculated by integrating the area between stimulation start and five seconds after cessation of stimulation of both stimulation blocks, after which the mean AUC was calculated (cumtrapz, MATLAB). Exclusion criteria were applied by excluding any mouse that was outside the outer fence using the interquartile range method. The AUCs of the ACC response (CFA, naïve, and  $\text{ACC}^{\text{CaMKII}}$ ) or S1BF (WP and WPOG) were used to calculate the outer fences. A final sample size was the following: CFA ( $n = 7/8$ ), naïve ( $n = 7/9$ ), WP/WPOG ( $n = 7/9$ ), and  $\text{ACC}^{\text{CaMKII}}$  ( $n = 6/7$ ). Comparison between two groups were conducted with GraphPad Prism. Statistical analyses of the AUC values were carried out using the Wilcoxon test or Mann-Whitney U test (one-tailed) as appropriate. For multiple comparisons, data were analyzed using the Kruskal-Wallis test followed by Dunn's multi test as appropriate.

### Functional connectivity analysis

Functional connectivity matrixes were made from calculating the Pearson correlation coefficient (MATLAB, corr) between all responsive ROIs ( $n = 40$ ), ipsilateral to ACC stimulation site, using the whole unsmoothed time series resulting in a 40 x 40 connectivity matrix for each animal. Matrixes were Fisher-z transformed for group-averaging and statistical tests. Results were converted back to  $r$  for presentation. The group connectivity matrix was further used to calculate modules using graph theory-based Newman's spectral

community detection via the Brain Connectivity Toolbox (BCT).<sup>99</sup> Modules refer to groups of nodes with high intra-connectivity and low inter-connectivity. As we only chose responsive ROIs, modularity was calculated with weighted, undirected matrixes. Resolution parameters were adjusted between 0.9 (larger modules) – 2 (smaller modules) until modularity values were maximized. CFA and naïve dataset did not result in logical modules with low modularity and thus was sorted based on anatomical groups. WP dataset resulted in two maximized modules using 0.9 resolution while WPOG dataset resulted in three modules with similar ordering to WP modules using 1.2 resolution. WPOG ROI ordering was shifted to match WP module ordering. Each subject matrix was reordered based on the calculated maximized module and unpaired (CFA vs naïve) or paired (WP vs WPOG) statistical testing using *network-based statistic* (NBS)<sup>100</sup> with a threshold of 2.3, 1,000 permutations, and significance of  $p=0.05$  after family-wise error rate multiple correction was conducted to find significant networks.